ELEKTRİK-ELEKTRONİK VE HABERLEŞME MÜHENDİSLİĞİ ALANINDA BİLİMSEL ARAŞTIRMALAR

Editör: Dr.Öğr.Üyesi Funda AKAR

yaz
yayınları

Elektrik-Elektronik ve Haberleşme Mühendisliği Alanında Bilimsel Araştırmalar

Editör

Dr.Öğr.Üyesi Funda AKAR

yaz yayınları

2026

yaz yayınları

Elektrik-Elektronik ve Haberleşme Mühendisliği Alanında Bilimsel Araştırmalar

Editör: Dr.Öğr.Üyesi Funda AKAR

E_ISBN 978-625-8574-70-8

Mart 2026 – Afyonkarahisar

Dizgi/Mizanpaj: YAZ Yayınları

Kapak Tasarım: YAZ Yayınları

YAZ Yayınları. Yayıncı Sertifika No: 73086

M.İhtisas OSB Mah. 4A Cad. No:3/3
İscehisar/AFYONKARAHİSAR

www.yazyayinlari.com

yazyayinlari@gmail.com

İÇİNDEKİLER

EVENT-TRIGGERED SLIDING MODE CONTROL: DESIGN PATTERNS, STABILITY LOGIC, AND SIMULATION-ORIENTED BENCHMARKING[1]

Ahmet ÇAKANEL[2]

1. INTRODUCTION

Sliding mode control (SMC) remains one of the most established robust control strategies in nonlinear systems engineering. Its long-standing appeal derives not from algorithmic complexity but from a structural property: the invariance of the sliding motion against matched disturbances under discontinuous control action (Utkin & Shi, 2017; Edwards & Spurgeon, 1998). This feature has sustained the relevance of SMC across diverse domains, including electromechanical drives, power converters, and networked cyber-physical systems, where model uncertainties are unavoidable.

In practice, however, sliding mode controllers are implemented digitally. Measurements are sampled, control laws are evaluated at discrete instants, and inputs are applied through zero-order holds. In networked or distributed settings, each control update consumes communication bandwidth and processing resources (Nešić & Teel, 2009; Heemels, Donkers, & Teel, 2013). Consequently, execution timing becomes an integral design dimension rather than a mere implementation detail.

---

[1] This chapter is an original and unpublished work and has not been derived from any thesis, conference paper, or previously published material.

[2] Assistant Professor, Kırklareli University, Faculty of Engineering, Department of Electrical-Electronics Engineering, ORCID: 0000-0003-2988-325X.

Conventional realizations employ periodic, time-triggered execution, where the controller updates at fixed sampling intervals regardless of the system's instantaneous state. While this simplifies scheduling and analysis, it does not distinguish between aggressive transient phases and near-equilibrium operation. As a result, computational effort may be expended even when corrective action is marginal.

Event-triggered control offers a state-dependent alternative. Instead of enforcing updates at every sampling instant, control actions are issued only when a predefined condition indicates that the current control input is no longer sufficiently accurate. Between two triggering instants, the previously computed input is retained. This mechanism concentrates updates during rapid state variations and naturally relaxes during steady operation. Its integration with sliding mode control has received increasing attention, as it promises substantial reduction in update density while preserving robustness characteristics (Wang, Han, & Ge, 2017; Li, Chen, & Huang, 2019; Zhang, Wang, & Li, 2021).

The present chapter examines event-triggered sliding mode control from an implementation-oriented perspective. Rather than proposing a new sliding law, the study isolates the effect of execution timing itself. Identical sliding surfaces, gains, and saturation limits are maintained across time-triggered and event-triggered realizations, so that any observed differences stem strictly from the update mechanism. Through a nonlinear benchmark and structured simulations, the analysis clarifies the practical trade-offs among tracking precision, control smoothness, and update frequency in digitally constrained environments.

2. BACKGROUND ON VARIABLE STRUCTURE SYSTEMS

Sliding mode control belongs to the broader class of variable structure systems (VSS), in which control laws switch according to system state. Consider a nonlinear system

$$\dot{x} = f(x) + g(x)u \tag{1}$$

where $x \in \mathbb{R}^n$ denotes the state vector, $u \in R$ is the control input, and $f(\cdot)$ and $g(\cdot)$ represent sufficiently smooth vector fields with sliding surface $s(x) = 0$. The control objective is to drive trajectories toward the manifold and maintain motion constrained to it.

A typical sliding control law adopts

$$u = u_{eq} - K\ sign(s) \tag{2}$$

where u_{eq} denotes the equivalent control term and $K > 0$ is a design gain. The discontinuous component ensures finite-time reachability provided that the reachability condition

$$s\dot{s} < 0 \tag{3}$$

is satisfied outside the sliding manifold. This inequality guarantees that the surface is attractive.

In digital implementations, discontinuous control is approximated through sample-and-hold execution, which affects switching density and practical robustness. Consequently, execution timing becomes relevant to sliding behavior.

3. FROM TIME-TRIGGERED TO EVENT-TRIGGERED CONTROL

Digital sliding mode implementations are typically time-triggered: measurements and control updates occur at fixed sampling intervals. This structure is predictable and easy to

schedule, but it applies corrections uniformly in time, regardless of system activity. As a result, updates continue even when the system operates near equilibrium and corrective action is minimal.

Event-triggered control replaces fixed periodic updates with state-dependent execution. The control input is recomputed only when a specified triggering condition is satisfied; otherwise, the previously calculated signal is maintained by a zero-order hold. The feedback law itself may remain unchanged—the modification lies entirely in the execution layer.

This shift concentrates computational effort during transients and reduces activity during steady operation. For sliding mode control, such timing variation affects how frequently the sliding variable is corrected, while preserving the underlying robustness mechanism. The next section formalizes this event-triggered structure for systematic comparison with periodic execution.

4. EVENT TIME-TRIGGERED SLIDING MODE CONTROL STRUCTURES

Event-triggered sliding mode control can be viewed as the meeting point of two ideas. One comes from sliding mode theory: robustness through discontinuous action. The other comes from digital control practice: update only when necessary. Bringing these two together is less about inventing a new control law and more about organizing how and when that law is applied.

Figure 1 illustrates the overall structure. The sliding mode controller itself is designed in continuous time, just as in a conventional implementation. What changes is the execution layer. Instead of updating at uniform sampling instants, the controller output is recomputed only when a triggering condition

is satisfied. Between events, the previous control value is held by a zero-order hold (ZOH).

A key design principle in this framework is the separation between the control law and the triggering mechanism. Keeping these two layers distinct has practical value. Existing sliding mode controllers can often be reused without structural redesign. Only the timing logic is modified. This modular approach simplifies experimental evaluation and makes comparisons between periodic and event-based realizations clearer. The triggering condition is typically formulated using measurable quantities. In sliding mode implementations, the sliding variable itself provides a natural candidate. It already encodes tracking error and system deviation in a compact way. Using it as the triggering signal aligns execution timing with the core control objective. When the system moves aggressively away from the manifold, events occur more frequently. When the trajectory remains within a small neighborhood of the surface, updates become sparse.

From an implementation standpoint, a distinction must be made between static and dynamic triggering rules. Static rules compare a measurable signal against a fixed threshold. They are transparent, easier to tune, and well-suited for benchmarking purposes. Dynamic triggers, in contrast, introduce internal states that evolve alongside the plant. While they may provide additional flexibility, they also increase parameter dependence and design complexity. For clarity and interpretability, the developments in this chapter adopt static triggering structures as the baseline configuration. Regardless of the chosen triggering logic, the physical interface with the plant relies on a zero-order hold. The control signal remains constant between two consecutive events. If the inter-event interval becomes large, this holding action may introduce visible deviations from ideal sliding motion. Conversely, very frequent events may approximate time-

triggered behavior. In this sense, execution timing directly shapes the apparent smoothness of the control effort.

To ensure feasibility on real hardware, triggering conditions are evaluated on a discrete-time grid. This avoids pathological behavior such as infinitely fast event sequences and reflects the finite resolution of digital platforms. The result is a structure that remains faithful to sliding mode principles while operating within realistic computational constraints.

5. SIMULATION BENCHMARK SYSTEM

To compare time-triggered and event-triggered sliding mode implementations under identical conditions, a common nonlinear benchmark is adopted throughout this study. The purpose of this benchmark is not to represent a particular industrial process, but to provide dynamics that are sufficiently nonlinear to expose implementation-level differences. The plant is a second-order nonlinear system of Duffing type. It captures linear damping, polynomial stiffness, and matched disturbances in a compact form that remains well suited for sliding mode design. The continuous-time model is defined as

$$\dot{x}_1(t) = x_2(t) \tag{4}$$

$$\dot{x}_2(t) = -ax_1(t) - bx_2(t) - cx_1^3 + u(t) + d(t) \tag{5}$$

where $x_1(t)$ and $x_2(t)$ are the system states, $u(t)$ is the control input, and $d(t)$ represents an external disturbance acting through the same channel as the control.

The measured output is assumed to be

$$y(t) = x_1(t) + n(t) \tag{6}$$

with $n(t)$ denoting measurement noise. This configuration corresponds to a matched uncertainty scenario, a

standard setting in sliding mode studies that allows robustness to be evaluated without auxiliary observer layers.

Unless stated otherwise, the nominal parameters are selected as

$$a = 1.0 \quad b = 0.6 \quad c = 0.2$$

which ensure stable open-loop behavior while preserving visible nonlinear effects. All simulations start from

$$x_1(0) = 0.8 \quad x_2(0) = 0$$

so that the initial deviation from the reference is nontrivial but not excessively large. The actuator is subject to saturation,

$$u(t) \in [-2.0, \quad 2.0]$$

and the same limits are imposed on all control strategies. The tracking objective is defined with respect to a smooth reference signal,

$$r(t) = 0.6 \ sin\, 0.5t + 0.2 \ sin\, 1.5t \tag{7}$$

which introduces both low- and moderate-frequency components. The corresponding tracking errors are

$$e_1(t) = x_1(t) - r(t) \tag{8}$$

$$e_2(t) = x_2(t) - \dot{r}(t) \tag{9}$$

These definitions allow a consistent construction of the sliding surface and ensure that both update strategies are evaluated against the same performance objective. To examine robustness, the system is subjected to a time-varying disturbance

$$d(t) = 0.3 \ sin\, 0.8t + 0.2 \ sin\, 2.2t \tag{10}$$

which provides persistent yet smooth perturbations. Measurement noise is modeled as zero-mean Gaussian noise,

$$n(t) \sim N(0, \sigma^2)$$

with a relatively small variance so that it perturbs the response without overwhelming the dynamics. No observers or filtering stages are introduced at this stage, since the intention is to compare intrinsic execution properties of the controllers under identical uncertainty conditions.

All simulations are performed using continuous-time numerical integration with a sufficiently small fixed integration step. Control decisions, however, are evaluated on a discrete-time grid. This base grid is shared by both implementations. In the time-triggered case, the control input is updated periodically according to a fixed sampling period. In the event-triggered case, the same grid is used to check the triggering condition; the control law is recomputed only when the condition is satisfied. Between updates, the control signal is maintained by a zero-order hold. This unified simulation structure guarantees that any performance differences originate from the triggering mechanism itself, rather than from inconsistencies in numerical integration or model representation.

6. SLIDING SURFACE AND CONTROL OBJECTIVE

A conventional first-order sliding surface is adopted:

$$s = \dot{e} + \lambda e \tag{11}$$

where $\lambda > 0$ determines convergence rate. The objective is to drive trajectories toward $s = 0$ and maintain them within a narrow neighborhood under disturbance and measurement noise.

The control structure is identical for both implementations and follows:

$$u = u_{eq} - K\ sat\left(\frac{s}{\phi}\right) \tag{12}$$

where u_{eq} compensates nominal dynamics, $K > 0$ ensures reachability, and ϕ defines a boundary layer to mitigate chattering. Actuator saturation limits are enforced uniformly.

The time-triggered implementation updates the control input at fixed sampling instants $t_k = kT_s$. Between sampling instants, the signal is held constant via a zero-order hold.

The event-triggered implementation evaluates a triggering condition on the same base grid. The control input is recomputed only when

$$|s(t_k) - s(t_{ki})| > \delta \tag{13}$$

where $\delta > 0$ is a design threshold and tkitki denotes the most recent update instant. Between events, the previously computed value is retained. Since the sliding surface and control gains are unchanged across both realizations, observed performance differences can be attributed solely to execution timing.

7. TIME-TRIGGERED SLIDING MODE CONTROLLER

The time-triggered sliding mode controller serves as the baseline configuration for all comparisons in this chapter. It follows the classical digital implementation principle: measure, compute, and update at fixed periodic instants. No state-dependent logic influences execution. This reflects standard industrial practice and provides a transparent point of reference before introducing event-based mechanisms. For the nonlinear benchmark system, the periodic control law is written as

$$u(t_k) = u_{eq}(t_k) - Ksign\left(s(t_k)\right) \tag{14}$$

where the sampling instants are defined as $t_k = kT_s$ with fixed sampling period T_s. The term u_{eq} compensates nominal

plant dynamics, while the discontinuous component scaled by $K > 0$ enforces robustness against matched disturbances. Once computed at time t_k, the control signal is held constant until the next sampling instant,

$$u(t) = u(t_k) \qquad t \in [t_k, t_{k+1}]$$

which introduces the familiar staircase profile associated with digital control. This sample-and-hold action already departs from ideal continuous switching. The sliding variable does not evolve under continuous corrective action, but under piecewise-constant inputs determined at discrete instants.

The sampling period T_s plays a central role. If chosen too small, the digital behavior approximates continuous-time sliding but increases processor load. If chosen too large, transient correction becomes coarse and oscillations around the manifold become more pronounced. For consistency, the same base sampling grid is later used to evaluate the triggering condition in the event-based case.

In practice, the discontinuous sign function may amplify measurement noise. To avoid unrealistic oscillations, a uniform smoothing mechanism—implemented as a boundary layer approximation— is applied consistently across all controllers. Similarly, actuator saturation limits are enforced directly on $u(t)$, without additional compensation schemes. This keeps the baseline intentionally simple and prevents secondary mechanisms from masking the influence of execution timing.

As a reference configuration, this time-triggered setup establishes measurable baselines for tracking accuracy, control smoothness, and update frequency. Any deviation observed in the subsequent sections can therefore be attributed to changes in the execution mechanism rather than alterations in the sliding law itself.

8. EVENT-TRIGGERED SLIDING MODE CONTROLLER

Unlike the periodic controller, the event-triggered scheme updates the control signal only when the system state justifies it. The sliding surface introduced earlier remains unchanged. So do the controller gains. What differs is not the control law itself, but the timing of its execution. The same discrete base sampling grid used in the time-triggered case is retained. At each grid instant, a triggering condition is evaluated. If the condition is satisfied, the control input is recomputed. If not, the previously applied value is maintained. This ensures that both implementations share an identical numerical backbone, so that any observed differences arise purely from update logic. Whenever an event is triggered at time t_k, the control law takes the familiar form in equation (12) which is structurally identical to the periodic law in (11). Between two triggering instants, the control input is held constant as before, where t_{k+1} now refers to the next event rather than a fixed sampling time.

The key element is therefore the triggering rule. A simple static condition is adopted. An update occurs whenever the change in the sliding variable since the last update exceeds a prescribed threshold:

$$|s(t) - s(t_k)| \geq \delta \tag{15}$$

where $\delta > 0$ defines the triggering sensitivity. Intuitively, this condition measures how far the system has drifted from the state at which the previous correction was computed. Small values of δ make the controller react frequently, producing behavior close to the periodic case. Larger values reduce the number of updates but allow a wider excursion of the sliding variable.

To prevent pathological behavior such as infinitely fast triggering, the condition is evaluated only on the discrete base

grid. This practical constraint introduces a natural minimum inter-event interval without requiring auxiliary dynamic trigger states or explicit dwell-time design. The objective here is not to construct the most sophisticated event-triggered scheme available in the literature. Instead, the emphasis is on clarity. By combining a standard sliding surface with a transparent static threshold rule, the comparison with the time-triggered controller remains interpretable. Any differences in tracking accuracy, control smoothness, or update density can therefore be attributed directly to the execution strategy rather than to architectural complexity.

9. PERFORMANCE METRICS AND COMPARATIVE RESULTS

This section compares the time-triggered and event-triggered sliding mode controllers under identical simulation conditions. The reference trajectory, disturbance signal, controller gains, and simulation length are kept exactly the same. The intention is simple: evaluate whether reducing update frequency alters tracking quality.

Several standard error metrics are used to quantify performance. Tracking accuracy is assessed using IAE, ISE, and RMSE. The maximum absolute tracking error is also reported to capture peak deviation. From an implementation perspective, the number of control updates and the mean inter-event time serve as indicators of execution effort.

Table 1. Tracking error metrics for time-triggered and event-triggered SMC.

Controller	IAE	ISE	RMSE	Max Error
TT-SMC	0.53	0.21	0.102	0.8075
ET-SMC	0.54	0.21	0.102	0.8078

Table 1 summarizes the tracking error metrics. Both controllers achieve nearly identical RMSE and ISE values. The

event-triggered implementation shows only a slight increase in IAE, while the maximum error remains practically unchanged. In other words, the reduction in updates does not translate into a visible degradation of tracking behavior.

Table 2 Execution metrics for time-triggered and event-triggered SMC.

Controller	Updates	MIET [s]	Update Reduction
TT-SMC	20,000	0.0010	-
ET-SMC	771	0.0259	96.1%

The execution-related differences, however, are substantial. Table 2 highlights this contrast. The time-triggered controller performs 20,000 updates, corresponding to periodic execution over the entire horizon. The event-triggered controller requires only 771 updates, which represents a reduction of more than 96%. The mean inter-event time of approximately 26 ms confirms that updates become sparse once the transient phase subsides.

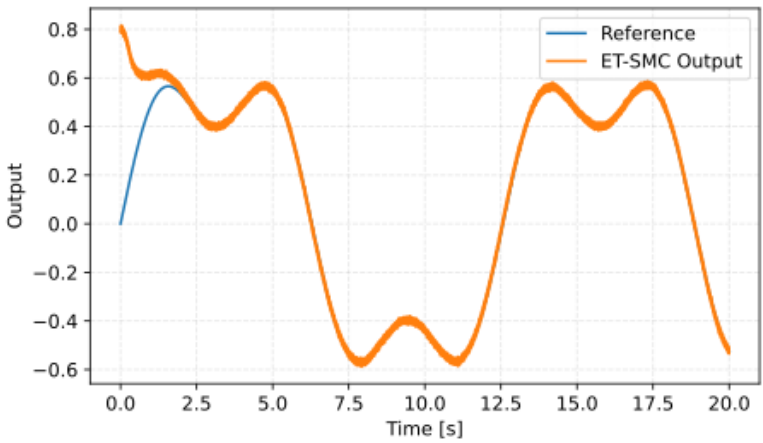

Figure 1. Reference tracking performance for the benchmark system.

The time-domain plots provide additional perspective. Figure 1 shows that both controllers track the reference closely.

No visible loss of accuracy is observed in the event-triggered case.

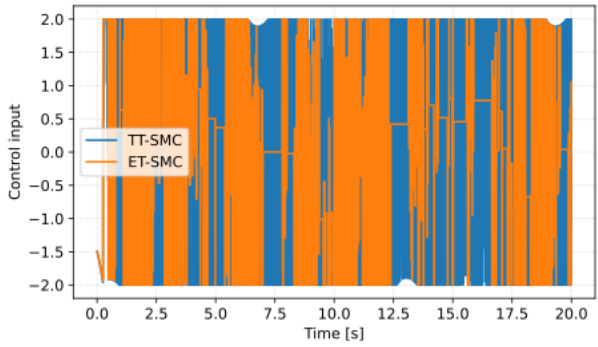

Figure 2. Control input signals for time-triggered and event-triggered SMC.

The corresponding control inputs appear in Figure 2. The periodic implementation produces uniformly spaced updates, while the event-triggered controller generates piecewise-constant segments of varying duration. Despite this structural difference, the overall amplitude range remains comparable.

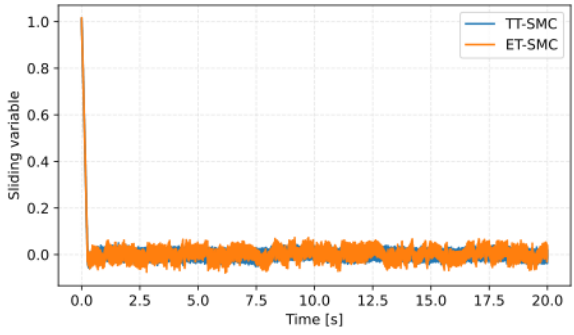

Figure 3. Sliding variable evolution under time-triggered and event-triggered execution.

Figure 3 illustrates the sliding variable. In both cases, trajectories converge toward a narrow band around zero. The event-based execution does not destroy the fundamental sliding

behavior. Instead, it relaxes how frequently corrective action is applied.

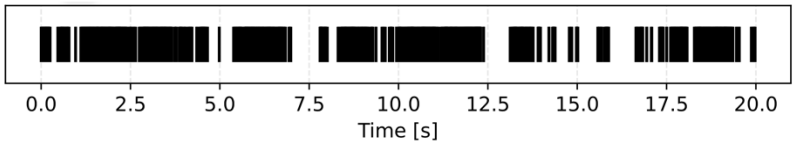

Figure 4. Triggering instants generated by the event-triggered sliding mode controller.

The adaptive nature of the event mechanism becomes clearer in Figure 4. Triggering events cluster during transients and become increasingly sparse during steady operation. This reflects the intended philosophy: update only when necessary.

The inter-event times shown in Figure 5 remain strictly positive. No vanishing intervals are observed, indicating that Zeno-like behavior does not arise for the selected threshold.

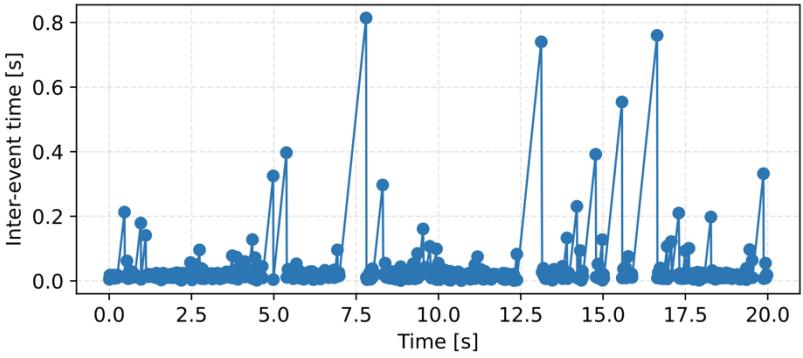

Figure 5. Evolution of inter-event times for the event-triggered sliding mode controller.

Taken together, the results suggest a clear outcome. Event-triggered sliding mode control preserves the essential tracking and robustness properties of its periodic counterpart, while dramatically reducing update frequency. In this benchmark setting, the change in execution timing brings efficiency gains without a meaningful loss in performance.

10. DISCUSSION: ENGINEERING INSIGHTS

The comparison demonstrates that execution timing directly influences computational demand while leaving tracking performance largely unchanged. The event-triggered controller concentrates updates during transients and substantially reduces activity in steady operation. In the benchmark scenario, update frequency decreases by more than 90% without a meaningful change in error metrics.

The triggering threshold defines the primary trade-off. Smaller thresholds approximate periodic execution and maintain tight sliding enforcement, whereas larger thresholds reduce update density at the cost of wider excursions around the sliding manifold. This balance must be selected according to application requirements rather than theoretical preference.

Overall, event-triggered sliding mode control should be interpreted as an execution-layer refinement rather than a structural redesign of sliding dynamics. Its benefits become particularly relevant in resource-constrained or networked environments where update density affects scalability, energy consumption, or communication load.

11. CONCLUSION AND FUTURE OUTLOOK

This chapter explored the effect of execution timing on sliding mode control within a unified nonlinear benchmark setting. The sliding surface, gains, and actuator limits were intentionally kept identical for both periodic and event-triggered implementations. This allowed the comparison to isolate one central question: what changes when only the update mechanism changes?

The results are clear. Event-triggered execution can reduce update frequency dramatically while preserving the core

tracking and disturbance rejection behavior associated with sliding mode control. In the presented benchmark, the reduction in updates exceeded ninety percent, yet the overall tracking quality remained nearly unchanged. The deviations that appeared were small and primarily confined to transient phases. At the same time, the study shows that execution timing is not neutral. Longer inter-event intervals slightly relax the tight enforcement of the sliding manifold. This reflects an inherent trade-off: precision is exchanged for computational and communication efficiency. Whether this exchange is acceptable depends on application demands rather than theoretical preference.

The analysis was intentionally kept simple. Matched disturbances and static triggering rules were considered to maintain architectural clarity. More complex environments— such as unmatched disturbances, network-induced delays, or higher-order sliding algorithms— may respond differently to irregular update timing. Threshold selection, in particular, remains an engineering choice that benefits from systematic simulation and practical experience.

Event-triggered sliding mode control should therefore be viewed not as a replacement for periodic sampling, but as a timing-layer refinement. Its relevance becomes especially evident in networked or resource-constrained systems, where update density directly affects scalability and energy usage. Future developments may include adaptive triggering mechanisms, data-driven threshold tuning, or integration with observer-based schemes. Such directions extend the ideas presented here, while keeping the central insight intact: in digital control, how often we act can matter almost as much as how we act.

REFERENCES

Bartolini, G., Ferrara, A., Levant, A., & Usai, E. (2015). A review on the application of second order sliding modes. *International Journal of Control, 88*, 1269–1294.

Edwards, C., & Spurgeon, S. K. (1998). Sliding mode control: Theory and applications. *Control Engineering Practice, 6*, 1435–1448.

Heemels, W. P. M. H., Donkers, M. C. F., & Teel, A. R. (2013). Periodic event-triggered control for linear systems. *IEEE Transactions on Automatic Control, 58*, 847–861.

Jiao, S., Liu, Y., & Zhang, H. (2023). Sliding mode control for networked control systems under DoS attacks via an event-triggered scheme. *Journal of the Franklin Institute, 360*, 2931–2954.

Li, Y., Chen, J., & Huang, B. (2019). Event-triggered dynamic sliding mode control for networked control systems. *IEEE Transactions on Industrial Electronics, 66*, 3120–3129.

Liu, C., Zhang, Y., & Chen, L. (2024). Dynamic event-triggered dual-channel quantized sliding mode control under DoS attacks. *Journal of the Franklin Institute, 361*.

Liu, Z., & Wang, J. (2018). Digital implementation issues in sliding mode control. *Annual Reviews in Control, 46*, 1–12.

Mazo, M., Jr., & Antsaklis, P. J. (2009). Systems over networks: Event-triggered control and reliability issues. *IEEE Transactions on Automatic Control, 54*, 1984–1998.

Meng, H., Zhang, J., & Li, S. (2024). Event-triggered predictive sliding mode control for discrete-time constrained systems. *International Journal of Robust and Nonlinear Control, 34*(2), 1358–1369.

Moheimani, S. O. R., Fleming, A. J., & Leang, K. K. (2021). Practical issues in the implementation of sliding mode control. *IEEE Control Systems Magazine*, *41*, 32–55.

Nešić, D., & Teel, A. R. (2009). A unified framework for design and analysis of networked control systems. *IEEE Transactions on Automatic Control*, *54*, 356–360.

Sarjaš, A., & Gleich, D. (2023). Event-triggered second-order sliding mode controller design and implementation. *Mathematics*, *11*(20).

Tabuada, P., Heemels, W., & Johansson, K. H. (2018). Event-triggered systems and applications: A tutorial. *IEEE Control Systems Magazine*, *38*, 45–75.

Utkin, V. I. (2019). Sliding modes after the first decade of the 21st century. *International Journal of Robust and Nonlinear Control*, *29*, 1483–1523.

Utkin, V. I., & Shi, J. (2017). *Sliding mode control: Theory and applications*. Boca Raton, FL: CRC Press.

Wang, L., Han, Q.-L., & Ge, S. S. (2017). Event-triggered sliding mode control of nonlinear systems via output feedback. *IEEE Transactions on Systems, Man, and Cybernetics: Systems*, *47*, 1291–1302.

Zhang, T., Wang, Y., & Li, X. (2021). Adaptive event-triggered sliding mode control with disturbance observer. *ISA Transactions*, *117*, 197–209.

Zhao, X., Meng, B., & Wang, Z. (2025). Event-triggered integral sliding mode control for uncertain networked systems. *International Journal of Systems Science*.

DISTURBANCE-AWARE SLIDING MODE CONTROL[1]

Ahmet ÇAKANEL[2]

1. DISTURBANCE ORIENTED PERSPECTIVE ON SLIDING MODE CONTROL

Robust control design often seeks structural mechanisms that preserve stability under uncertainty. Among such mechanisms, sliding mode control occupies a distinctive position. Its principal appeal lies in its ability to maintain acceptable performance in the presence of matched uncertainties and disturbances, particularly when these disturbances enter through the control channel (Edwards & Spurgeon, 1998; Utkin, 2019). For this reason, SMC has been applied across diverse domains including motion systems, power electronics, aerospace platforms, and electromechanical drives.

In its classical geometric interpretation, sliding mode control enforces a predefined manifold in the state space. Once sliding motion is established, reduced-order dynamics become largely insensitive to matched uncertainties (Utkin, 2017). While this invariance property remains central to the theory, practical implementations reveal a more nuanced signal-level behavior. In digitally implemented controllers, switching action not only preserves the sliding condition but also implicitly compensates

[1] This chapter is an original and unpublished work and has not been derived from any thesis, conference paper, or previously published material.

[2] Assistant Professor, Kırklareli University, Faculty of Engineering, Department of Electrical-Electronics Engineering, ORCID: 0000-0003-2988-325X.

for modeling errors, parameter variation, actuator limits, and measurement imperfections.

From this viewpoint, the switching term plays a dual role. It enforces sliding motion while simultaneously absorbing unmodeled effects. When uncertainty is persistent or slowly varying, this compensation burden may lead to visibly active control signals. Although stability is preserved, the resulting control effort may appear unnecessarily aggressive in practice, particularly in sampled implementations (Bartolini, Ferrara, & Usai, 2015). This observation motivates reconsidering how disturbance compensation is distributed within the control structure.

A useful way to reinterpret sliding mode control is through the concept of equivalent control. Under ideal sliding conditions, the equivalent control represents the continuous input that maintains motion on the manifold (Utkin, 2017). In the presence of disturbances, this component implicitly reflects both nominal dynamics and disturbance effects. The switching term then adjusts around this implicit baseline. Disturbance rejection is therefore achieved, but compensation is not explicitly separated from robust enforcement.

These considerations motivate the introduction of disturbance awareness. Rather than relying exclusively on switching to counteract uncertainty, a disturbance-aware structure attempts to reconstruct part of the unknown influence and incorporate it explicitly into the control loop. The objective is not to replace the inherent robustness of sliding mode control. Instead, it is to redistribute part of the compensation effort away from discontinuous action and toward a structured internal estimate.

Disturbances are typically modeled in lumped form, aggregating external loads, parametric uncertainty, and

unmodeled nonlinear dynamics into a single unknown term. In matched configurations, this lumped disturbance enters through the same channel as the control input, preserving the robustness framework of classical SMC while enabling explicit estimation.

Three estimation paradigms appear frequently in disturbance-aware sliding mode studies. The extended state observer (ESO) augments the plant model with an additional state capturing aggregated disturbance effects and reconstructs this state online (Zhang, Guo, & Song, 2022; Zhang & Chen, 2021). Active disturbance rejection control (ADRC) adopts a disturbance-centric philosophy in which unknown effects are estimated and compensated directly within the control law (Aguilar-Orduña & Castillo, 2020). Sliding-mode-based observers exploit discontinuous dynamics and finite-time convergence properties to estimate unknown inputs or disturbances (Zhao, Li, & Wang, 2021). Although mathematically distinct, these approaches share a structural objective: to make uncertainty partially explicit rather than leaving it entirely embedded within the switching mechanism.

Disturbance estimation does not eliminate robustness concerns. Observer bandwidth selection introduces trade-offs between responsiveness and noise sensitivity. Aggressive estimation may amplify measurement noise, whereas conservative tuning may delay compensation (Zhang et al., 2022). Thus, disturbance awareness modifies the distribution of robustness rather than removing its necessity.

The purpose of this chapter is not to introduce a new control law. Instead, it examines representative disturbance-aware sliding mode control architectures under a common nonlinear benchmark. By comparing baseline and observer-augmented structures within identical conditions, the chapter aims to clarify how explicit disturbance estimation influences

tracking behavior, control smoothness, and tuning considerations in practice.

2. OBSERVER-AUGMENTED SLIDING MODE STRUCTURES

Disturbance-aware sliding mode control modifies the internal structure of the control loop by introducing an explicit estimation pathway. While baseline sliding mode control compensates uncertainty implicitly through switching, observer-augmented architectures aim to reconstruct part of the disturbance and incorporate this estimate directly into the control signal.

Figure 1 illustrates the generic structure considered in this chapter. In the baseline configuration, plant outputs feed directly into the sliding surface, and uncertainty is addressed exclusively through the switching term. In disturbance-aware variants, an observer reconstructs a lumped disturbance signal using available measurements. This estimate is then injected into the control law, effectively redefining how uncertainty compensation is distributed within the loop.

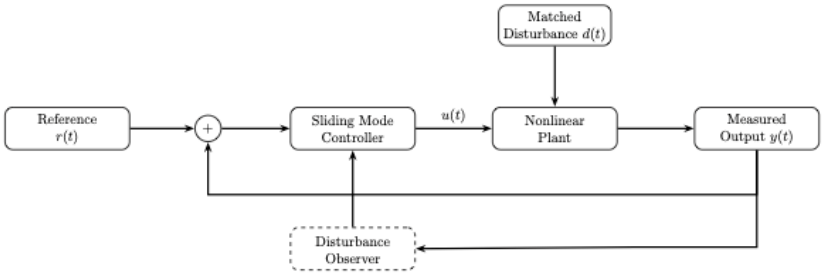

Figure 1. Generic structure of baseline and observer-augmented sliding mode control. The observer block reconstructs a lumped disturbance estimate that modifies the control input while preserving the sliding structure.

The most common estimation paradigm is the extended state observer (ESO), in which the plant model is augmented with

an additional state representing aggregated disturbance effects. The reconstructed disturbance is subtracted from the nominal control component, allowing the switching mechanism to operate within a reduced uncertainty envelope. This structure preserves the original sliding surface while redistributing compensation effort.

Active disturbance rejection formulations adopt a disturbance-centric perspective, treating uncertainty as a generalized signal to be estimated and rejected explicitly. When combined with sliding mode control, this viewpoint emphasizes estimation-driven compensation while retaining switching as a robustness safeguard.

Sliding-mode-based observers constitute a more tightly integrated alternative. These observers exploit discontinuous dynamics and finite-time convergence properties to estimate disturbances or unknown inputs. Their convergence can be rapid, but noise sensitivity must be managed carefully through smoothing or boundary-layer techniques.

Architecturally, all considered disturbance-aware structures share a common objective: separate disturbance reconstruction from sliding enforcement. The distinction lies not in whether uncertainty is compensated, but in how explicitly that compensation is represented. ESO-based designs emphasize modular separation between observer and controller. Sliding-mode observers embed estimation within discontinuous dynamics. Higher-order sliding mode variants introduce additional internal dynamics to improve smoothness while maintaining robustness.

From a design standpoint, this structural modification changes the distribution of tuning effort. Baseline SMC relies primarily on switching gain selection to guarantee robustness. Observer-augmented designs introduce additional parameters

governing estimation bandwidth and noise sensitivity. These parameters interact with control gains but also provide finer adjustment of signal-level behavior.

The architectures examined in this chapter preserve the fundamental matched-disturbance robustness of sliding mode control. The purpose of augmentation is not to replace invariance properties, but to influence how control effort is expressed in practice, particularly under persistent or structured disturbances.

3. SIMULATION BENCHMARK SYSTEM

The objective of the present chapter is not to demonstrate numerical superiority of a particular observer design, but to interpret how explicit disturbance estimation reshapes the expression of robustness in sliding mode control. For this purpose, a nonlinear simulation framework is employed as an analytical instrument rather than as a performance showcase.

The adopted plant model is intentionally selected to remain structurally simple while preserving nonlinear behavior. It captures the essential ingredients required for meaningful sliding mode analysis: nonlinear state dynamics, matched disturbance injection, and bounded control authority. The system is second order and exhibits nonlinear stiffness together with damping effects. This combination allows disturbance-induced deviations to manifest clearly without introducing excessive modeling complexity.

A lumped disturbance enters through the same channel as the control input. This matched structure is deliberate. Classical sliding mode theory already guarantees invariance properties under matched uncertainty. Therefore, any observable difference between baseline and observer-augmented configurations cannot be attributed to a loss of theoretical robustness. Instead,

differences must arise from how disturbance information is processed and redistributed within the control architecture.

The measured output is assumed to be affected by low-level noise. The magnitude of this perturbation is selected such that it does not dominate the disturbance dynamics, yet remains sufficient to reveal estimation–noise trade-offs when observers are introduced. No additional filtering stages are incorporated beyond those intrinsic to the examined architectures, so that noise sensitivity remains visible in its natural form.

3.1. Reference Trajectory and Excitation Philosophy

The control objective is defined as bounded reference tracking. The chosen reference trajectory contains multiple frequency components so that both slow and moderately varying system responses are excited. This ensures that disturbance compensation mechanisms are exercised across different dynamic regimes rather than being evaluated under a single operating condition.

The disturbance signal is constructed as a smooth yet persistent perturbation composed of multiple frequency components. The emphasis is not on abrupt or impulsive excitation, but on structured uncertainty that challenges sustained compensation. This profile allows one to observe whether disturbance effects are absorbed implicitly by switching activity or explicitly by estimation mechanisms.

By avoiding extreme or pathological disturbance scenarios, the framework maintains interpretability. The intent is not to push the controller to instability limits, but to observe how robustness manifests at the signal level under realistic and persistent uncertainty.

3.2. Numerical Consistency Across Architectures

All controller variants are evaluated under an identical numerical framework. The same plant realization, disturbance signal, and reference trajectory are applied to each architecture. Differences in behavior therefore stem exclusively from structural modifications within the control loop.

Actuator saturation limits are enforced uniformly, and no additional compensation mechanisms (e.g., anti-windup schemes) are introduced. This ensures that observed differences reflect architectural redistribution of disturbance compensation rather than auxiliary mechanisms.

4. COMPARATIVE PERFORMANCE EVALUATION

This section examines how different disturbance-aware sliding mode architectures express robustness at the signal level. The purpose is not to establish numerical superiority, but to interpret how the redistribution of disturbance compensation influences observable behavior. All considered configurations operate within a common structural setting so that architectural differences, rather than modeling variations, explain the observed distinctions. The discussion therefore emphasizes trends and qualitative patterns rather than isolated quantitative metrics.

4.1. Interpreting Tracking Behavior

Across configurations, stable reference tracking is preserved. This outcome is consistent with the matched-disturbance framework of sliding mode theory, which guarantees invariance properties under appropriate gain selection. The introduction of explicit disturbance estimation does not alter this fundamental guarantee. What changes is the manner in which robustness is manifested. In baseline sliding mode control,

uncertainty is absorbed predominantly through switching activity. In observer-augmented structures, part of the disturbance influence is compensated through the estimation layer before it reaches the switching mechanism.

From an architectural standpoint, tracking precision therefore reflects not only the sliding surface design, but also the internal allocation of compensation effort. In the examined scenarios, performance differences remain modest, indicating that estimation enhances signal distribution rather than redefining stability properties.

4.2. Disturbance Estimation as Structural Redistribution

The disturbance estimate serves as a structural mediator between uncertainty and control action. Rather than being eliminated, disturbance effects are reconstructed and explicitly incorporated into the control loop. ESO-based structures tend to exhibit smoother disturbance reconstructions, reflecting bandwidth-limited estimation. Sliding-mode-based observers respond more aggressively, often achieving rapid convergence at the cost of increased sensitivity to measurement noise. These differences do not fundamentally alter robustness, but they reshape how it becomes visible in the control signal.

The key architectural insight is that explicit estimation modifies *where* compensation occurs. Baseline SMC concentrates corrective effort in the discontinuous term. Observer-augmented SMC shares this burden between the estimation layer and the switching component.

4.3. Control Signal Expression and Smoothness

The most visible distinction between architectures appears in the control signal. In the absence of disturbance estimation, the switching term carries the primary responsibility for

counteracting uncertainty. This can lead to visibly active control behavior under persistent disturbances. When a disturbance estimate is available, part of this activity is absorbed internally before it manifests as switching intensity. The control signal may therefore appear smoother, even though the underlying robustness properties remain unchanged. This redistribution is particularly noticeable under slowly varying or bias-like disturbances. Under rapidly changing conditions, estimation limits become more apparent, and differences between architectures diminish.

4.4. Practical Implementation Perspective

From an implementation standpoint, disturbance-aware structures introduce additional internal dynamics associated with estimation. These dynamics increase algorithmic complexity, but they also provide interpretability. The estimated disturbance becomes an observable signal that can guide tuning decisions and diagnostic reasoning. Importantly, disturbance estimation does not inherently reduce computational execution requirements. Its primary impact lies in signal-level redistribution of robustness rather than in update sparsification. This distinction separates disturbance-aware architectures from execution-oriented refinements such as event-triggered control. Taken together, the observations suggest that observer augmentation does not redefine sliding mode robustness; instead, it reshapes its practical expression.

4. DISCUSSION: PRACTICAL ROBUSTNESS INSIGHTS

The comparative results presented in the previous section offer an opportunity to reflect on disturbance-aware sliding mode control from a practical engineering perspective. Rather than focusing on numerical superiority, this discussion emphasizes

how different architectural choices influence control behavior, tuning effort, and interpretability. These aspects often play a decisive role in real-world applications, even when formal performance metrics appear similar, particularly in digitally implemented systems.

4.1. When Disturbance Awareness is Beneficial

The simulations indicate that explicit disturbance estimation can be advantageous in scenarios where disturbances exhibit persistent or slowly varying components. In such cases, observer-augmented architectures redistribute part of the compensation task away from the switching mechanism. The resulting control signals tend to exhibit reduced variation over time, which may be desirable in systems sensitive to actuator wear or mechanical stress, as also observed in applied disturbance-aware SMC studies. This benefit does not imply that disturbance-aware designs outperform baseline sliding mode control in all circumstances. When disturbances change rapidly or measurement noise dominates, the added estimation layer may offer limited improvement. Under these conditions, the intrinsic robustness of sliding mode control already provides a strong level of disturbance rejection, consistent with classical robustness interpretations.

From an application standpoint, disturbance awareness is best viewed as an enhancement rather than a replacement. Its value depends on the nature of uncertainty, the available sensing quality, and the priorities of the control task.

4.2. Tuning Effort and Design Transparency

Introducing a disturbance observer reshapes the tuning landscape. In baseline sliding mode control, robustness margins are often enforced by selecting a sufficiently large switching gain. This choice is straightforward but may lead to conservative behavior, particularly when uncertainty is persistent.

Observer-augmented designs introduce additional parameters that influence performance. Observer bandwidth, correction gains, and smoothing mechanisms must be selected alongside control gains. While this increases design effort, it also enables more targeted adjustments. Uncertainty compensation can be addressed explicitly through observer tuning rather than implicitly through aggressive switching, a shift often highlighted in disturbance-aware control frameworks.

Design transparency is an important consideration here. Architectures that expose the disturbance estimate as an accessible signal support diagnostic reasoning. Engineers can inspect the estimate, assess its plausibility, and adjust parameters accordingly. This transparency can be valuable during commissioning and troubleshooting.

4.3. Noise Sensitivity and Bandwidth Trade-Offs

All disturbance estimation techniques rely on assumptions regarding signal smoothness and noise characteristics. Increasing observer bandwidth improves responsiveness but may amplify measurement noise. Reducing bandwidth improves noise robustness at the cost of delayed estimation.

These trade-offs are neither unique to a particular observer design nor easily eliminated. Instead, they must be balanced in a context-dependent manner. The simulation results suggest that moderate observer tuning often yields the most balanced behavior, avoiding both excessive noise amplification and sluggish disturbance tracking. It is also worth noting that noise sensitivity manifests differently across architectures. ESO-based designs tend to smooth disturbance estimates naturally. Sliding-mode-based observers respond more sharply, which can be advantageous in low-noise settings but problematic otherwise. These tendencies should be considered during controller selection.

4.4. Implications for Implementation-Oriented Design

From an implementation perspective, the choice between baseline and disturbance-aware sliding mode control is rarely binary. In many systems, a simple SMC design may already meet performance requirements. In others, excessive control activity or limited interpretability may motivate the introduction of disturbance estimation.

The results presented in this chapter suggest that observer-augmented SMC structures can provide meaningful benefits without altering the fundamental robustness properties of sliding mode control. At the same time, they introduce additional design degrees of freedom that must be managed carefully. Ultimately, the most appropriate architecture depends on application-specific constraints. Computational resources, sensing quality, actuator limitations, and performance priorities all influence the decision. Simulation-based evaluation, as employed here, remains a practical and effective tool for exploring these trade-offs before committing to hardware implementation.

5. CONCLUSIONS AND RESEARCH OUTLOOK

This chapter examined disturbance-aware sliding mode control from an architectural and implementation-oriented perspective. No new control laws or observer formulations were introduced. Instead, the focus was placed on how explicit disturbance estimation alters the practical behavior and interpretation of sliding mode control. Baseline SMC and observer-augmented variants were considered within a common nonlinear benchmark under matched disturbance conditions, allowing structural differences to be observed under comparable assumptions.

The simulation results indicate that incorporating disturbance estimation does not alter the fundamental robustness traditionally associated with sliding mode control. Stable reference tracking is preserved across all examined architectures. What changes is the manner in which robustness is expressed at the signal level. When a disturbance estimate is available, part of the compensation effort shifts away from the switching action toward the estimation layer. This redistribution affects control smoothness, tuning emphasis, and the visibility of internal signals.

Several practical observations follow from this comparison. Observer-augmented structures often exhibit less visibly aggressive control behavior when disturbances vary slowly or contain bias-like components. They also provide auxiliary signals that can assist during tuning and commissioning. At the same time, these benefits introduce additional considerations. Observer bandwidth selection, noise sensitivity, and interaction with the control loop require careful attention. Across the studied scenarios, no single architecture emerges as uniformly preferable.

From an engineering standpoint, disturbance-aware sliding mode control is best viewed as an optional enhancement rather than a default solution. In applications where a baseline SMC design already meets performance and implementation requirements, additional estimation layers may offer limited benefit. In contrast, when persistent disturbances, excessive control activity, or limited interpretability are concerns, observer augmentation can provide meaningful advantages.

The scope of the chapter was intentionally limited. Only matched disturbances were considered, and the benchmark system was selected for clarity rather than realism. Extensions to unmatched uncertainty, measurement delays, or networked

implementations remain open topics. Further investigation of higher-order sliding mode controllers and adaptive or gain-scheduled observers is also warranted, particularly in discrete-time and embedded settings.

Another possible direction involves data-assisted or learning-based disturbance estimation. Such methods may complement classical observers by adapting to changing conditions over time. Any such extension, however, must be approached cautiously to preserve the interpretability and robustness that motivate the use of sliding mode control in the first place.

Overall, this chapter is intended as a practical reference rather than a prescriptive guide. By emphasizing architectural clarity and simulation-based observation, it aims to support informed and context-aware design choices when combining sliding mode control with explicit disturbance estimation.

REFERENCES

Aguilar-Orduña, M., & Castillo, R. (2020). Active disturbance rejection control: Overview and perspectives. *IFAC-PapersOnLine, 53*(2), 110–115. https://doi.org/10.1016/j.ifacol.2020.12.020

Alsubaie, H., et al. (2023). Disturbance observer-based terminal sliding mode control for nanobeams. *Mathematics, 11*(3), 789. https://doi.org/10.3390/math11030789

Bartolini, G., Ferrara, A., & Usai, E. (2015). Chattering avoidance by second-order sliding mode control. *IEEE Transactions on Automatic Control, 43*(2), 241–246.

Chang, S., Liu, H., & Zhang, Y. (2024). Sliding mode disturbance observer for optical inertial platforms. *Machines, 12*(12), 849. https://doi.org/10.3390/machines12120849

Edwards, C., & Spurgeon, S. K. (1998). *Sliding mode control: Theory and applications*. Taylor & Francis.

Gu, J., Wang, X., & Li, Y. (2024). Observer-based adaptive sliding mode compensation under lumped disturbances. *Sensors, 24*(8), 2404. https://doi.org/10.3390/s24082404

Guo, K., Zhang, H., & Wei, C. (2024). Sliding mode control with nonlinear disturbance observer for robotic manipulators. *Scientific Reports, 14*, 30656. https://doi.org/10.1038/s41598-024-77125-y

Liu, Y., Laghrouche, S., & Depernet, D. (2023). Super-twisting sliding-mode observer-based control for PMSM drives. *Journal of the Franklin Institute, 360*(1), 985–1004. https://doi.org/10.1016/j.jfranklin.2022.12.014

Luo, M., Zhang, X., & Liu, Y. (2023). Adaptive sliding mode control with ESO for high-speed PMSM. *Scientific*

Reports, 13, 33455. https://doi.org/10.1038/s41598-023-33455-x

Ran, C., Wu, X., & Zhang, Y. (2023). Event-triggered sliding-mode control with disturbance estimation. *International Journal of Control, 96*(9), 2031–2045. https://doi.org/10.1080/00207179.2022.2032363

Shi, X., Cheng, Y., & Yin, C. (2024). Disturbance-observer-assisted sliding mode control for steer-by-wire systems. *Vehicle System Dynamics, 62*(6), 1921–1942. https://doi.org/10.1080/00423114.2024.2305296

Sun, Z., Liu, X., & Chen, Y. (2024). Disturbance observer-based fixed-time sliding mode control for elevator systems. *Actuators, 13*(11), 438. https://doi.org/10.3390/act13110438

Utkin, V. I. (2017). Sliding mode control. In *Springer handbook of automation* (pp. 577–591). Springer.

Utkin, V. I. (2019). *Sliding modes in control and optimization*. Springer.

Zhang, Y., & Chen, J. (2021). Observer-augmented sliding mode control for uncertain nonlinear systems. *Automatica, 132*, 109606. https://doi.org/10.1016/j.automatica.2021.109606

Zhang, Z., Guo, Y., & Song, X. (2022). Improved nonlinear extended state observer-based sliding-mode control for hydraulic systems. *Entropy, 24*(1), 41. https://doi.org/10.3390/e24010041

Zhao, J., Li, Y., & Wang, H. (2021). Disturbance observer aided super-twisting sliding mode control. *Mechatronics, 78*, 102554. https://doi.org/10.1016/j.mechatronics.2021.102554

Zheng, R., Zhu, Q., & Huang, S. (2024). ESO-based sliding-mode control for tight aircraft formation. *Drones*, *8*(4), 165. https://doi.org/10.3390/drones8040165

SLIDING MODE BASED SELF-OPTIMIZATION: DESIGN PRINCIPLES AND NUMERICAL ILLUSTRATION[1]

Ahmet ÇAKANEL[2]

Vadim I. UTKIN[3]

1. INTRODUCTION

Optimization is an inherent objective in many control applications. In a number of practical systems, the desired operating condition is not specified as a fixed reference value. Instead, it corresponds to an extremum of a performance function that may be only partially known. In such cases, regulation and search must coexist. The controller implicitly performs both tasks.

Extremum-seeking control has addressed this problem for several decades (Krstić & Wang, 2000; Ariyur & Krstić, 2003; Tan, Nešić, & Mareels, 2006). Classical approaches typically rely on gradient information. The gradient may be calculated analytically, estimated numerically, or reconstructed via probing signals. Periodic perturbations and averaging analysis are often involved (Krstić & Wang, 2000; Ariyur & Krstić, 2003; Tan, Nešić, & Mareels, 2006). These methods have been used

---

[1] This chapter is based in part on the doctoral dissertation entitled "Self-Optimization Systems Design Based on Sliding Mode Control", completed by Ahmet Çakanel at The Ohio State University, Department of Electrical and Computer Engineering, 2017. The material has been reorganized and adapted for the present format.

[2] Assistant Professor, Kırklareli University, Faculty of Engineering, Department of Electrical-Electronics Engineering, ORCID: 0000-0003-2988-325X.

[3] Professor, Department of Electrical and Computer Engineering, The Ohio State University, Columbus, OH, USA. †Deceased, 2022.

successfully in many applications. Nevertheless, practical implementation may require additional signal injection, filtering, and parameter tuning. Near an extremum, the gradient magnitude naturally decreases. Convergence may slow down. Sensitivity to disturbances may increase.

Sliding Mode Control (SMC) offers a different perspective. Its primary domain has been regulation and tracking problems under uncertainty (Utkin, 1977; Utkin, 2013; Edwards & Spurgeon, 1998; Shtessel et al., 2014). The approach employs discontinuous control actions to enforce motion on a predefined manifold. Robustness with respect to matched disturbances is a well-documented property. The method is not traditionally associated with extremum-seeking. Still, the underlying mechanism allows an alternative interpretation.

In sliding-mode-based self-optimization, the extremum search is reformulated as a tracking problem with a monotonic reference signal. The reference evolves in a single direction. The plant output is forced to follow it. As long as feasibility conditions are satisfied, the state evolves toward the extremum region. No explicit gradient measurement is required. The switching structure replaces direct derivative evaluation.

Accuracy in such a framework is not arbitrarily adjustable. When the trajectory approaches the extremum, ideal sliding motion cannot persist in continuous form. A bounded oscillatory regime appears. Its amplitude is related to the hysteresis implementation. This feature does not represent a failure of the method; rather, it defines its practical resolution.

The aim of this chapter is to present the method from a design-oriented viewpoint. The emphasis is on structural properties. Formal proofs are not repeated in full detail. Instead, selected elements are revisited in a compact form, followed by a simple numerical illustration. The example serves to demonstrate

parameter influence and switching behavior. No global optimality claim is made.

2. SELF OPTIMIZATION PROBLEM FORMULATION

Consider a dynamical plant whose steady-state behavior may be expressed in the form

$$y = f(x) \tag{1}$$

where $x \in \mathbb{R}$ represents an adjustable input and $y \in \mathbb{R}$ denotes a measurable performance output. The objective of self-optimization is to steer the system toward an extremum point x^* satisfying

$$f'(x^*) = 0 \tag{2}$$

while relying solely on measurements of y. This optimality condition is standard in steady-state optimization theory (Khalil & Grizzle, 2002; Boyd & Vandenberghe, 2004). In the present context, however, the explicit form of $f(x)$ is not assumed to be available.

In practical systems the function $f(x)$ may be partially known, poorly identified, or affected by disturbances. Even when an approximate model exists, gradient information can be sensitive to uncertainty. Instead of computing or estimating $f'(x)$ directly, one may seek a mechanism that drives x toward the extremum using information that emerges from closed-loop interaction. The viewpoint adopted here does not begin with gradient reconstruction. It begins with a tracking structure.

To that end, introduce a reference signal g(t) that varies monotonically according to

$$\dot{g}(t) = -\rho, \qquad \rho > 0 \tag{3}$$

Define the tracking error

$$\varepsilon(t) = g(t) - y(t) \tag{4}$$

The optimization task is reformulated as enforcing $\varepsilon \to 0$. If the output follows a decreasing reference, the associated input x evolves in a direction consistent with local descent as long as the plant gain does not change sign. The mechanism is indirect. The system is not told where the extremum is located. It is instead compelled to follow a moving reference whose monotonic evolution induces directional motion in the input space.

Within this interpretation, extremum seeking becomes a special case of a tracking problem with a structured reference. The adjustment variable x is governed by

$$\dot{x} = u, \qquad u = -A\, sign(\varepsilon) \tag{5}$$

where $A > 0$ is a constant design parameter. Discontinuous control of this type is standard in sliding-mode design (Utkin, 1977; Levant, 2003). The switching action attempts to drive the error toward the manifold $\varepsilon = 0$. When reachability conditions are satisfied, a sliding-type motion occurs in the output space.

Ideal discontinuities are not physically realizable. In implementation, switching is performed with a finite hysteresis band. Let $\Delta > 0$ denote half of the hysteresis width. The control changes sign only when ε crosses $\pm\Delta$. This modification prevents infinitely fast switching and introduces a finite oscillatory region near the sliding manifold. The presence of the hysteresis band is not merely a practical detail. It defines the neighborhood in which the search process eventually settles.

As the trajectory approaches the extremum, the local gradient $f'(x)$ decreases in magnitude. The sliding condition may no longer be satisfied in an ideal sense. The closed-loop dynamics then transition into a bounded oscillatory regime. The amplitude

of this oscillation depends on the hysteresis parameter and on the chosen gain A. Exact convergence to x^* in continuous time is therefore not expected under practical switching. Instead, a finite-resolution neighborhood is obtained.

Figure 1 illustrates the overall structure of the proposed scheme.

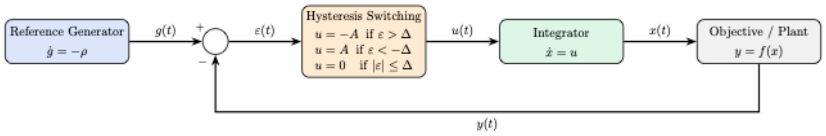

Figure 1. Block diagram of the sliding-mode-based self-optimization scheme. A monotonically decreasing reference $g(t)$ is generated with slope ρ. The tracking error $\varepsilon = g - y$ is processed through a hysteresis-based switching block. The resulting discontinuous control signal u drives the integrator that updates the search variable x.

The reference generator produces the monotonic signal $g(t)$, and the plant output $y = f(x)$ follows this trajectory through switching action. The direction of optimization emerges from the interaction between the plant's local gain and the sign of the tracking error. No explicit gradient evaluation block is required. The search process is therefore embedded in the closed-loop structure itself.

3. SLIDING MODE BASED SEARCH MECHANISM

The search mechanism follows directly from the tracking structure introduced earlier. The switching law is driven by the error $\varepsilon = g(t) - y(t)$, and the resulting motion in x is obtained through integration of the discontinuous signal u. To examine the behavior more closely, consider the time derivative of the error

$$\dot{\varepsilon} = \dot{g} - \dot{y} \tag{6}$$

Assuming that the plant output satisfies $\dot{y} = f'(x)\,\dot{x}$ and using $\dot{x} = u$, the error dynamics may be expressed as

$$\dot{\varepsilon} = -\rho - f'(x)u \tag{7}$$

With the control law

$$u = -A\,sign(\varepsilon) \tag{8}$$

the dynamics of the tracking error become

$$\dot{\varepsilon} = -\rho + Af'(x)sign(\varepsilon) \tag{9}$$

The existence of sliding motion on the surface $\varepsilon = 0$ follows under the condition

$$A|f'(x)| > \rho \tag{10}$$

This inequality is analogous to the classical reachability requirement in sliding mode theory (Utkin, 2013; Shtessel et al., 2014). When it holds, the error is driven toward zero from both sides of the manifold. The plant output therefore follows the decreasing reference, and the variable x evolves in a direction compatible with descent of the objective function. The directional information is not computed explicitly. It appears through the interaction between the plant gain $f'(x)$ and the sign of ε.

As the state approaches the extremum region, the magnitude of $f'(x)$ reduces. The inequality $A|f'(x)| > \rho$ may then cease to hold. At that point ideal sliding motion cannot be maintained. The system does not converge to a fixed equilibrium in the classical sense. Instead, the trajectory remains in a bounded neighborhood. This loss of ideal sliding near points where the gain vanishes is consistent with established observations in sliding mode analysis (Levant, 1993, 2003). It does not contradict the mechanism. It defines its limitation.

In practice, discontinuous switching is implemented through hysteresis. Let 2Δ denote the band width. The control reverses sign when ε crosses $\pm\Delta$. The effect is twofold. First, the switching frequency becomes finite and measurable. Second, the closed-loop trajectory develops a steady oscillatory regime. The oscillations are centered near the extremum, and their amplitude depends on both Δ and the local gradient slope. The motion is alternating. It is not stationary in an exact sense. However, its mean position remains near the extremum region.

One important point follows from this structure. The achievable accuracy is not arbitrarily small unless Δ is reduced. Decreasing Δ narrows the oscillatory neighborhood. At the same time, switching activity increases. The design trade-off is therefore explicit. Precision is improved at the expense of higher switching density. This balance is typical in practical sliding mode implementations and does not require additional gradient reconstruction. Viewed in this manner, sliding-mode-based self-optimization can be interpreted as a sign-driven adjustment process. The extremum is not identified through algebraic differentiation. It is approached through enforced oscillatory motion whose average drift is governed by the interaction of the plant gain and the reference slope. The mechanism is structural rather than algorithmic.

4. ACCURACY AND ROLE OF THE HYSTERESIS BAND

When the condition $A|f'(x)| > \rho$ ceases to hold near the extremum, ideal sliding motion cannot be sustained. The system does not settle at a fixed equilibrium. Instead, it evolves within a small oscillatory region whose size is determined primarily by the hysteresis band used in switching. Inside the band $|\varepsilon| \leq \Delta$, the control alternates between two constant values. During one half-

cycle the input x increases, and during the other it decreases. Because the gradient $f'(x)$ is not symmetric around the extremum, the increments in x on either side are not identical. On one side the gradient magnitude is relatively larger. Closer to the extremum it diminishes. This imbalance introduces a slow average drift toward the optimal region while individual cycles generate bounded oscillations.

As the extremum is approached more closely, the magnitude of the gradient decreases further. The oscillatory regime becomes more pronounced relative to the local slope. Exact convergence is therefore not expected in practice when hysteresis is present. The trajectory remains confined within a finite neighborhood. The width of this neighborhood is governed by Δ together with the local gain.

A simple estimate may be obtained by noting that each switching cycle corresponds to a traversal of approximately 2Δ in the error variable. The associated variation in the input x is therefore proportional to Δ scaled by the inverse of the local gradient magnitude. From this observation it follows that the steady-state deviation from the true extremum is of order Δ. The approximation is qualitative, yet it captures the dominant dependence.

The reference slope ρ influences how quickly the search progresses during transients. It does not by itself determine the final resolution. Even with a small ρ, the oscillatory band persists if Δ is finite. Conversely, reducing Δ narrows the steady-state neighborhood but increases switching activity. The trade-off appears directly in the structure. Higher resolution requires more frequent sign changes.

In implementation, the choice of Δ is therefore practical. Very small values may lead to excessive switching in the presence of measurement noise or sampling limitations. Larger values

improve robustness but reduce attainable precision. The oscillatory behavior near the extremum is not incidental. It reflects the finite switching mechanism. Within this framework it defines the achievable accuracy of the self-optimization process.

5. NUMERICAL ILLUSTRATION

To examine the structural properties of the proposed scheme, consider the nonlinear scalar function

$$f(x) = (x - 1.5)^2 + 0.2(x - 1.5)^3 \qquad (11)$$

which possesses a single minimum near $x^* = 1.5$. The cubic term introduces mild asymmetry so that the gradients on either side of the extremum are not identical. This avoids the symmetry of a purely quadratic test function and produces slightly different local slopes in ascent and descent directions.

The variable x is updated through the discontinuous law developed earlier. The output is defined as $y = f(x)$, and the reference evolves according to $\dot{g} = -\rho$. Switching is implemented with a hysteresis band $|\varepsilon| \leq \Delta$. All simulations were carried out in discrete time with fixed integration step.

Two initial conditions were considered. The first case uses $x_0 = -0.5$, which lies on the descending side of the objective function. The second case uses $x_0 = 3.0$, which lies beyond the minimum on the opposite slope. The objective here is not comparative benchmarking, but observation of structural behavior.

Table 1 Design-oriented sweep results in the steady oscillatory regime ($x_0 = -0.5$). All steady-state quantities are computed over the final simulation interval

Δ	$\bar{x}$	A_x	RMS(ε)	N_{sw}	$\overline{T}_{IET}[ms]$
0.03	-0.1223	0.085	0.0260	168	35.714
0.02	-0.1169	0.085	0.0162	170	35.294
0.01	-0.1103	0.090	0.0064	174	34.483
0.006	-0.1079	0.085	0.0031	174	34.483
0.004	-0.1067	0.085	0.0024	306	19.608

Here, $\bar{x}$ denotes the steady-state mean value of the search variable, Ax represents the oscillation amplitude of x in steady state, N_{sw} is the total number of switching events observed, and $\overline{T}_{IET}$denotes the mean inter-event time.

For $x_0 = -0.5$, the system evolves toward a bounded oscillatory regime. Table 1 reports steady-state quantities for several values of Δ. As Δ decreases from 0.03 to 0.004, the RMS tracking error decreases from approximately 0.026 to 0.0024. The steady-state mean of x shifts gradually, while remaining in a confined neighborhood. The oscillation amplitude remains bounded. Switching activity increases as the band narrows. For the smallest band width considered, the number of switching events approximately doubles compared to the largest band. The trend follows directly from the relay structure.

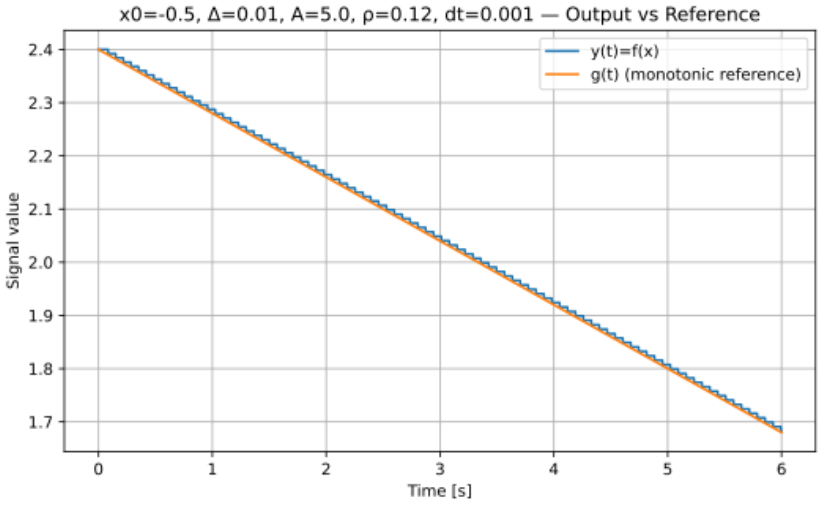

Figure 2. Output $\mathbf{y(t)}$ and reference $\mathbf{g(t)}$ for $\Delta = \mathbf{0.01}$, $\mathbf{x_0 = -0.5}$

Figure 2 shows representative trajectories of $y(t)$ and $g(t)$ for $\Delta = 0.01$ with $x_0 = -0.5$. After the initial transient, the output follows the monotonic reference with small oscillations. The bounded nature of the steady state is visible. Figure 3 presents a magnified portion of the switching signal. The control alternates between two finite values. No excessively rapid toggling appears in this example.

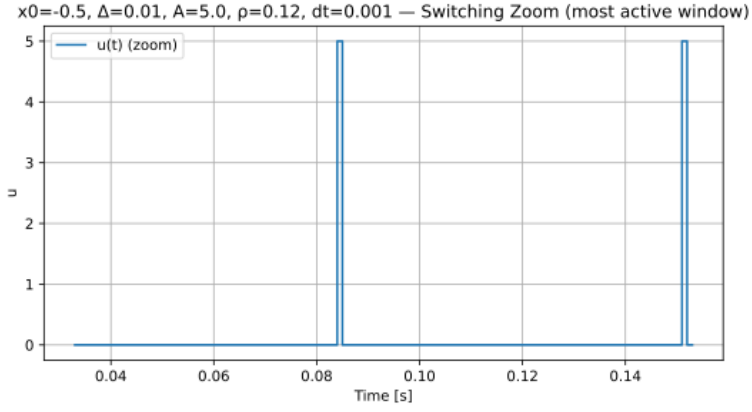

Figure 3. Zoomed segment of switching signal $u(t)$ for $\Delta = \mathbf{0.01}$, $x\mathbf{0} = -\mathbf{0.5}$.

The dependence of steady-state accuracy on Δ is shown directly in Figure 4. The decrease in RMS tracking error with decreasing hysteresis width is clearly visible. The relationship is not perfectly linear, which reflects the influence of the local gradient. Nevertheless, the dominant dependence remains evident.

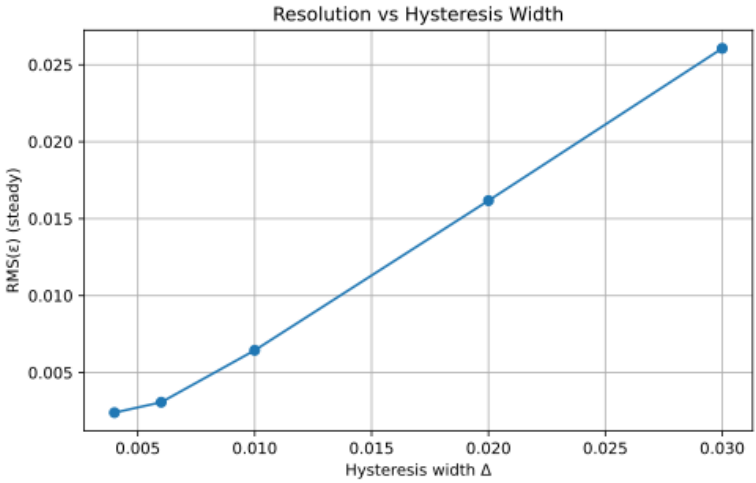

Figure 4. Steady-state RMS tracking error as a function of hysteresis width.

When the initial condition is changed to $x_0 = 3.0$, a different behavior is obtained. The trajectory does not enter an oscillatory regime around the extremum. After a single switching event, the state moves monotonically in one direction. The mean value grows significantly within the simulation interval. Figure 5 illustrates this case. The monotonic nature of the reference and the absence of gradient sign correction led to departure from the extremum basin.

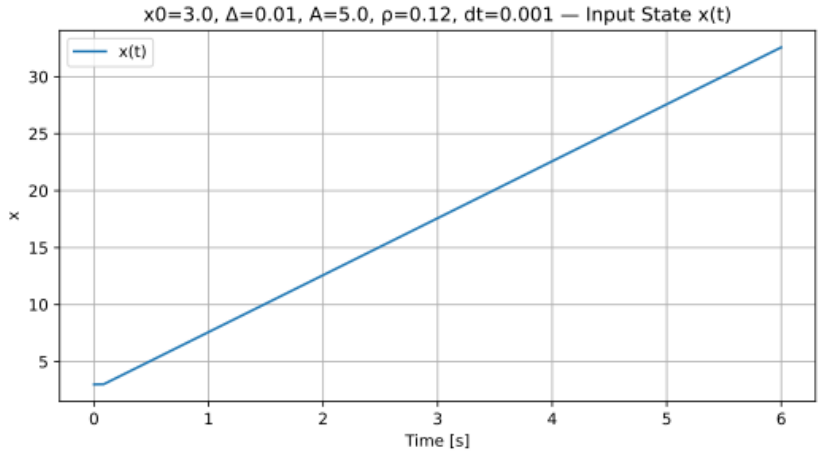

Figure 5. State trajectory for $x_0 = 3.0$ with $\Delta = 0.01$.

Two structural features are therefore apparent. The first concerns attainable steady-state accuracy, which depends primarily on the hysteresis width. The second concerns basin dependence. The method does not guarantee global convergence from arbitrary initial conditions. Within the appropriate region of the objective function, bounded oscillatory motion around the extremum is observed. Outside that region, the trajectory may move away from the minimum.

6. DISCUSSION

The preceding development examined sliding-mode-based self-optimization as a gradient-free search mechanism built around a discontinuous tracking structure. The essential feature is that directional information is not computed explicitly. No analytical differentiation is performed. Instead, the sign of the tracking error, combined with the plant's local gain, determines the motion in the input space. When reachability conditions are satisfied, the closed-loop system exhibits a sliding-type behavior in the output variable. The search appears as a consequence of this interaction.

Near the extremum, the gradient magnitude decreases. The classical sliding inequality cannot be maintained arbitrarily close to the minimum. The system then evolves within a bounded oscillatory region. This transition does not indicate instability. It reflects the finite implementation of discontinuous control. The hysteresis width introduces a resolution scale. Reducing Δ contracts the neighborhood around the extremum, but switching activity increases accordingly. The relationship is direct and can be observed numerically in the preceding section.

The reference slope ρ influences how rapidly the search progresses during transients. It does not determine the final steady-state accuracy on its own. That accuracy is tied more closely to the hysteresis band and the local gradient magnitude. The control gain A affects the robustness margin of the reachability condition. Very large gains are not necessary in the simple scalar example presented here, yet the parameter remains relevant in uncertain or higher-order systems.

When compared conceptually to classical extremum-seeking schemes that employ probing or dithering signals (Krstić & Wang, 2000; Ariyur & Krstić, 2003; Tan, Nešić, & Mareels, 2006; Stanković & Stipanović, 2010; Dochain, Perrier, & Guay, 2011), the present formulation avoids the need for injected high-frequency excitation and additional filtering stages. At the same time, both approaches share an important limitation. Under realistic switching or sampling constraints, convergence to the exact extremum is not achieved in finite time. Practical operation is characterized by bounded motion around the optimal region.

The numerical illustration also indicates that convergence is not global with respect to the initial condition. The reference is monotonic and does not adapt its direction. If the initial state lies outside the region in which the gradient sign is compatible with the enforced tracking condition, the trajectory may not approach

the extremum. In this sense, the method should be viewed as a structured local search mechanism rather than a universal optimization solver.

From an implementation perspective, the formulation remains relatively simple. The algorithm requires measurement of the performance output and realization of a relay-type switching law. No gradient reconstruction block appears in the structure. This may be advantageous in applications where modeling uncertainty is significant or where computational simplicity is preferred. Sliding-mode-based self-optimization therefore occupies a distinct position among gradient-free techniques. Its defining characteristics are robustness, structural simplicity, and a resolution determined explicitly by switching design choices.

7. CONCLUSION

This chapter examined sliding-mode-based self-optimization from a design-oriented viewpoint. The extremum-seeking task was reformulated as a tracking problem driven by a monotonic reference signal. Within this structure, directional motion toward the extremum emerges without explicit gradient evaluation. The control law remains discontinuous, and its implementation through hysteresis determines the steady-state behavior.

The analysis indicates that attainable accuracy is closely linked to the switching band. The reference slope influences how rapidly the state approaches the extremum region during transients. Near the optimum, the gradient magnitude decreases and ideal sliding motion cannot persist in continuous form. A bounded oscillatory regime appears instead. Its amplitude scales with the hysteresis width and the local gain. This behavior is not

incidental; it defines the finite resolution of the method under practical switching.

The numerical illustration showed these structural properties in a simple scalar example. For initial conditions within the appropriate basin, the system entered a bounded oscillatory motion around the extremum region. When the initial condition was chosen outside that region, convergence was not observed. The method therefore operates as a local search mechanism. It does not claim global optimality.

Despite its conceptual simplicity, the approach offers an alternative to schemes that rely on gradient reconstruction or high-frequency probing. Implementation requires only measurement of the performance output and a relay-type switching law. The resulting behavior reflects a compromise. Convergence speed, robustness, and switching activity are linked through the switching design. The framework may serve as a starting point for further extensions in systems where the operating point must be adjusted during operation and detailed analytical models are not readily available.

REFERENCES

Ariyur, K. B., & Krstić, M. (2003). *Real-time optimization by extremum-seeking control*. Wiley.

Behera, A. K., Bandyopadhyay, B., Cucuzzella, M., Ferrara, A., & Yu, X. (2021). A survey on event-triggered sliding mode control. *IEEE Journal of Emerging and Selected Topics in Industrial Electronics, 2*(3), 206–217.

Boyd, S., & Vandenberghe, L. (2004). *Convex optimization*. Cambridge University Press.

Castellanos-Cárdenas, D., Posada, N. L., Orozco-Duque, A., Sepúlveda-Cano, L. M., Castrillón, F., Camacho, O. E., & Vásquez, R. E. (2024). A review on data-driven model-free sliding mode control. *Algorithms, 17*(12), 543.

Dochain, D., Perrier, M., & Guay, M. (2011). Extremum seeking control and its application to process and reaction systems: A survey. *Mathematics and Computers in Simulation, 82*(3), 369–380.

Edwards, C., & Spurgeon, S. K. (1998). *Sliding mode control: Theory and applications*. CRC Press.

Khalil, H. K., & Grizzle, J. W. (2002). *Nonlinear systems* (3rd ed.). Prentice Hall.

Korovin, S. K., & Utkin, V. I. (1974). Using sliding modes in static optimization and nonlinear programming. *Automatica, 10*(5), 525–532.

Krstić, M. (2000). Performance improvement and limitations in extremum seeking control. *Systems & Control Letters, 39*(5), 313–326.

Krstić, M., & Wang, H. H. (2000). Stability of extremum seeking feedback for general nonlinear dynamic systems. *Automatica, 36*(4), 595–601.

Kumari, K., Bandyopadhyay, B., Reger, J., & Behera, A. K. (2020). Event-triggered sliding mode control for a high-order system via reduced-order model-based design. *Automatica, 121,* 109163.

Levant, A. (1993). Sliding order and sliding accuracy in sliding mode control. *International Journal of Control, 58*(6), 1247–1263.

Levant, A. (2003). Higher-order sliding modes, differentiation and output-feedback control. *International Journal of Control, 76*(9–10), 924–941.

Moreno, J. A., & Fridman, L. (2023). A survey on high-order sliding-mode control design using Lyapunov functions. *IFAC-PapersOnLine, 56*(2), 25–36.

Moreno, J. A., & Osorio, M. (2012). Strict Lyapunov functions for the super-twisting algorithm. *IEEE Transactions on Automatic Control, 57*(4), 1035–1040.

Oliveira, T. R., Peixoto, A. J., & Hsu, L. (2012). Global real-time optimization by output-feedback extremum-seeking control with sliding modes. *Journal of the Franklin Institute, 349*(4), 1397–1415.

Pan, Y., & Özgüner, Ü. (2004). Sliding mode extremum seeking control for linear quadratic dynamic game. In *Proceedings of the American Control Conference* (pp. 614–619). IEEE.

Pan, Y., Acarman, T., & Özgüner, Ü. (2002). Nash solution by extremum seeking control approach. In *Proceedings of the IEEE Conference on Decision and Control* (pp. 329–334).

Pan, Y., Özgüner, Ü., & Acarman, T. (2003). Stability and performance improvement of extremum seeking control

with sliding mode. *International Journal of Control, 76*(9–10), 968–985.

Polyakov, A., & Fridman, L. (2014). Stability notions and Lyapunov functions for sliding mode control systems. *Journal of the Franklin Institute, 351*(4), 1831–1865.

Scheinker, A. (2024). 100 years of extremum seeking: A survey. *Automatica, 161*, 111481.

Shtessel, Y., Edwards, C., Fridman, L., & Levant, A. (2014). *Sliding mode control and observation*. Birkhäuser.

Slotine, J. J. E., & Li, W. (1991). *Applied nonlinear control*. Prentice Hall.

Stanković, M. S., & Stipanović, D. M. (2010). Extremum seeking under stochastic noise and applications to mobile sensors. *Automatica, 46*(8), 1243–1251.

Tan, Y., Moase, W. H., Manzie, C., Nešić, D., & Mareels, I. M. (2010). Extremum seeking from 1922 to 2010. In *Proceedings of the 29th Chinese Control Conference* (pp. 14–26). IEEE.

Tan, Y., Nešić, D., & Mareels, I. (2006). On non-local stability properties of extremum seeking control. *Automatica, 42*(6), 889–903.

Utkin, V. I. (1977). Variable structure systems with sliding modes. *IEEE Transactions on Automatic Control, 22*(2), 212–222.

Utkin, V. I. (2013). *Sliding modes in control and optimization*. Springer.

Utkin, V., Poznyak, A., Orlov, Y., & Polyakov, A. (2020). Conventional and high-order sliding mode

control. *Journal of the Franklin Institute, 357*(15), 10244–10261.

Wu, L., Liu, J., Vazquez, S., & Mazumder, S. K. (2021). Sliding mode control in power converters and drives: A review. *IEEE/CAA Journal of Automatica Sinica, 9*(3), 392–406.

Xiao, H., Zhao, D., Gao, S., & Spurgeon, S. K. (2022). Sliding mode predictive control: A survey. *Annual Reviews in Control, 54*, 148–166.

Yu, H., & Özgüner, Ü. (2002). Extremum-seeking control via sliding mode with periodic search signals. In *Proceedings of the 41st IEEE Conference on Decision and Control* (pp. 323–328). IEEE.

Yu, H., & Özgüner, Ü. (2003). Smooth extremum-seeking control via second-order sliding mode. In *Proceedings of the American Control Conference* (pp. 3248–3253). IEEE.

Zhang, C., & Ordonez, R. (2007). Numerical optimization-based extremum seeking control with application to ABS design. *IEEE Transactions on Automatic Control, 52*(3), 454–467.

Zhao, Z., Li, Y., Salsbury, T. I., House, J. M., & Alcala, C. F. (2020). Local self-optimizing control based on extremum seeking control. *Control Engineering Practice, 99*, 104394.

SEZGİSEL OPTİMİZASYON ALGORİTMALARI KULLANILARAK PEMFC MODELLERİNİN KARŞILAŞTIRMALI PARAMETRE TAHMİNİ

Mustafa SAKA[1]

Melih ÇOBAN[2]

1. GİRİŞ

Küresel enerji talebinin sürekli artması, geleneksel fosil yakıt rezervlerinin hızla tükenmesi ve çevresel kirliliğin azaltılmasına yönelik acil ihtiyaç, sürdürülebilir ve temiz enerji çözümlerine yönelik arayışı yoğunlaştırmıştır. Bu bağlamda, hidrojen, yüksek dönüşüm verimliliği, çevre dostu olması ve çok yönlülüğü nedeniyle en umut vadeden enerji taşıyıcılarından biri olarak ortaya çıkmıştır. Hidrojen bazlı enerji sistemlerine geçiş, özellikle toplam enerji tüketiminin ve sera gazı emisyonlarının önemli bir bölümünü oluşturan kentsel bölgelerde daha da artmaktadır (Xu vd., 2019).

Hidrojen enerji dönüşüm teknolojileri arasında, hidrojenin kimyasal enerjisini minimum çevresel etkiyle doğrudan elektrik enerjisine dönüştürebilen verimli elektrokimyasal cihazlar olarak yakıt hücreleri öne çıkmaktadır. Özellikle proton değişim membranlı yakıt hücreleri (PEMFC), yüksek güç yoğunluğu, üstün verimlilik, düşük çalışma sıcaklığı, hızlı başlatma yeteneği, kompakt yapısı, düşük gürültü emisyonu ve elverişli dinamik

[1] Doç. Dr., İskenderun Teknik Üniversitesi, Mühendislik ve Doğa Bilimleri Fakültesi, Elektrik Elektronik Mühendisliği, ORCID: 0000-0003-4157-2980.

[2] Dr. Öğr. Üyesi, Bolu Abant İzzet Baysal Üniversitesi, Mühendislik Fakültesi, Elektrik Elektronik Mühendisliği, ORCID: 0000-0001-9528-7187.

tepkisi nedeniyle önemli bir araştırma konusu olmuştur. Bu ayırt edici özellikler, PEMFC'leri yüksek enerji yoğunluğunun ve kritik gereksinimlerin olduğu ulaşım sistemleri de dahil olmak üzere geniş bir uygulama yelpazesi için son derece önemli kılar. Avantajlarına rağmen, PEMFC'ler karmaşık dinamik davranış sergilerler. Bu davranışlar arasındaki etkileşim, doğru performans analizi, sistem optimizasyonu ve gelişmiş kontrol tasarımı için önemli zorluklar oluşturur. Sonuç olarak, PEMFC sistemlerinin güvenilir bir şekilde matematiksel modellenmesi, iç fiziksel süreçleri anlamada ve verimliliği artırmada çok önemli bir rol oynar (Menesy vd., 2025).

PEMFC modellemesi, çıkış gerilimi ve akım yoğunluğu arasındaki ilişkiyi tanımlayan polarizasyon eğrisinin doğru bir şekilde karakterize edilmesine odaklanır. Bu eğri, birden fazla iç kayıp ve çalışma koşulunun birleşik etkilerini kapsar. Basitlikleri ve hesaplama verimlilikleri nedeniyle, bu amaçla ampirik ve yarı ampirik modeller yaygın olarak kullanılmaktadır. Ancak, bu modeller, yüksek modelleme doğruluğunu sağlamak için doğru tahmin edilmesi şart olan birçok bilinmeyen parametre içermektedir. PEMFC sistemlerinde parametre tanımlama, optimizasyon ortamının doğrusal olmayan, çok değişkenli ve çok modlu doğası nedeniyle zordur ve genellikle birden fazla yerel optimuma yol açar. Geleneksel optimizasyon teknikleri, bu koşullar altında tatmin edici tahmin doğruluğu ve sağlamlığı elde etmekte sıklıkla başarısız olmaktadır. Bu nedenle, sezgisel optimizasyon algoritmalarına dayalı gelişmiş parametre tahmin yöntemleri son yıllarda giderek artan bir ilgi görmektedir. Bu teknikler, gelişmiş küresel arama yeteneği, iyileştirilmiş yakınsama özellikleri ve doğrusal olmayan optimizasyon problemlerine üstün uyarlanabilirlik sunmaktadır. PEMFC model parametrelerinin doğru bir şekilde tanımlanmasıyla, sistem modelleme hassasiyetini, performans tahminini, arıza teşhisini ve gerçek zamanlı kontrol stratejilerini önemli ölçüde iyileştirmek

mümkün hale gelir. Bu bağlamda, sağlam ve verimli parametre tahmin çerçeveleri geliştirmek, PEMFC teknolojilerinin pratik olarak uygulanmasını ve büyük ölçekli ticarileştirilmesini hızlandırmak için kritik öneme sahiptir (Ayyaro vd., 2024).

PEMFC sistemlerinin doğrusal olmayan, çok değişkenli ve karmaşık yapısı, parametre tahmin problemini zorlu bir optimizasyon problemi hâline getirmekte ve klasik yöntemlerin bu tür problemlerde yetersiz kaldığını göstermektedir. Bu nedenle, literatürde meta-sezgisel ve hibrit optimizasyon algoritmalarına dayalı pek çok yenilikçi yaklaşım önerilmiştir (Ayyaro vd., 2024; Rezk vd., 2022; Hachana & El-Fergany 2022).

(Mbasso vd., 2025) yaptıkları çalışmada küresel arama ve yerel iyileştirme yeteneklerini dengeleyen hibrit bir meta-sezgisel yöntem olan HBASCSO algoritması geliştirilmiş ve altı farklı PEMFC yığını üzerinde test edilmiştir. Önerilen yöntem, PSO, DE ve GWO gibi geleneksel algoritmalara kıyasla %90'ın üzerinde yakınsama hızı artışı ve %70'e varan tahmin hatası azalması sağlamıştır. Benzer şekilde, çalışma (El-Fergany, 2018)' de Salp Swarm Optimizer (SSO) tabanlı bir yaklaşım kullanılarak PEMFC modelinin bilinmeyen parametreleri toplam karesel sapma (TSD) minimizasyonu yoluyla başarıyla tahmin edilmiştir. NedStack PS6 ve BCS 500 W PEMFC sistemleri üzerinde gerçekleştirilen çalışmalar, önerilen yöntemin yüksek doğruluk, hızlı yakınsama ve literatürdeki diğer algoritmalara göre üstün performans sergilediğini göstermiştir (El-Fergany, 2018). Moth Search Algorithm (MSA) temelli bir başka çalışmada, PEMFC parametre tahmini problemi için yeni bir optimizasyon çerçevesi sunulmuş ve yöntemin etkinliği iki farklı test sistemi üzerinde doğrulanmıştır. Çalışmada, deneysel ve hesaplanan gerilim değerleri arasındaki toplam karesel fark minimize edilerek yüksek model uyumu elde edilmiş, ayrıca önerilen algoritmanın mevcut literatürdeki yöntemlere göre daha kararlı sonuçlar sunduğu rapor edilmiştir (Sun, Su, Yin, & Jermsittiparsert, 2020).

(Menesy vd., 2025) yaptıkları çaloşmada ise Electric Eel Foraging Optimization (EEFO) algoritması kullanılarak PEMFC parametre tahmini gerçekleştirilmiş ve dört farklı ticari PEMFC sistemi üzerinde doğrulanmıştır. Sonuçlar, EEFO algoritmasının yüksek doğruluk, hızlı yakınsama ve güçlü kararlılık sunduğunu, ayrıca hesaplama yükünü azaltan indirgenmiş parametreli modellerle yüksek uyum sağlandığını göstermiştir (Menesy vd., 2025).

Bu çalışma kapsamında, PEMFC modelinin parametre tahmini problemi üç farklı sezgisel optimizasyon yöntemi (Zebra Optimizasyon Algoritması, Altın Çakal Optimizasyon Algoritması ve Dhole Optimizasyon Algoritması) kullanılarak ele alınmıştır. Her bir algoritmanın performansı karşılaştırmalı olarak değerlendirilmiş ve elde edilen sonuçlar üzerinden yöntemler analiz edilmiştir. Böylece, PEMFC parametre tahmini problemi için en uygun optimizasyon yaklaşımının belirlenmesi amaçlanmıştır.

2. PEMFC'nin MATEMATİKSEL MODELLENMESİ

PEMFC, hidrojen ve oksijenin kimyasal enerjisini katalitik reaksiyonlar yoluyla doğrudan elektrik enerjisine dönüştüren elektrokimyasal bir cihazdır. Hücre, bir anot, bir katot ve bir proton değişim membranı (PEM) içerirken, akış kanalları reaksiyon gazlarını katalizör katmanlarına sağlar. Anotta, hidrojen proton ve elektronlara ayrışır. Protonlar PEM üzerinden katoda doğru hareket ederken, elektronlar harici bir devre üzerinden hareket ederek elektrik akımı üretir. Katotta, oksijen proton ve elektronlarla birleşerek su ve ısı üretir.

PEMFC'nin açık devre voltajını simüle etmek için genellikle Nernst denklemi (E_n) kullanılır. Bu denklem (1) (Mbasso vd., 2025) ile formüle edilir.

$$E_n = 1.229 - 0.85 \times 10^{-3}\left(T_f - 298.15\right) + 4.3085 \times 10^{-5} \times T_f \times \ln\left(P_{H_2}\sqrt{P_{O_2}}\right) \quad (1)$$

T_f (K) hücrenin sıcaklığını gösterirken, P_{H_2} ve P_{O_2} sırasıyla H_2 ve O_2 kısmi basınçlarını (atm) ifade etmektedir. PEMFC'leri oluşturan üç tip aşırı potansiyel vardır. Birincisi düşük akımda aktivasyon voltajı (V_{act}), ikincisi membran direncinin bir fonksiyonu olarak ifade edilen Ohmik direnç düşüşü (V_R) ve üçüncüsü konsantrasyon aşırı potansiyelidir (V_{conc}). Bu voltaj düşüşleri sırasıyla aşağıdaki denklemlerdeki gibi ifade edilebilirler.

$$V_{act} = -[\xi_1 + \xi_2 T_f + \xi_3 T_f \ln\left(C_{O_2}\right) + \xi_4 T_f \ln\left(I_f\right)] \quad (2)$$

$$C_{O_2} = \frac{P_{O_2}}{5.08\times10^6} \times e^{\frac{-498}{T_f}} \quad (3)$$

$$V_R = I_f(R_m + R_c),\ R_m = \frac{\rho_m \times l}{A} \quad (4)$$

$$\rho_m = \frac{181.6[1+0.03\left(\frac{I_f}{A}\right)+0.062(\frac{T_f}{303})^2\times(\frac{I_f}{A})^{2.5}]}{[\gamma-0.634-3\left(\frac{I_f}{A}\right)9]e^{4.18\frac{T_f-303}{T_f}}} \quad (5)$$

$$V_{conc} = -\beta \ln\left(\frac{j_{max}-j}{j_{max}}\right) \quad (6)$$

C_{O_2} oksijen konsantrasyonunu ifade etmektedir. $\xi_1, \ldots \xi_4$ değerleri optimizasyon tekniği ile tahmin edilen parametrelerdir. R_m ve R_c sırasıyla membran ve bağlantı dirençlerini göstermektedir. ρ_m membran öz direncini, l membran kalınlığını ve A membran alanını β ve γ ayarlanabilir parametreleri ifade etmektedir. j_{max} ise maksimum akım yoğunluğudur. Daha yüksek gerilim elde edebilmek için hücreler seri bağlanmaktadır. Seri bağlanmış hücre yığının gerilim aşağıdaki gibi ifade edilebilmektedir.

$$V_{stack} = N_{cells} \times (E_n - V_{act} - V_R - V_{conc}) \quad (7)$$

Burada, N_{cells} hücre sayısını göstermektedir. Üreticiler tarafından kullanıcılara sunulmayan parametreler ($\xi_1,\ldots \xi_4, R_c, \beta$) optimizasyon algoritmaları tarafından en iyi şekilde tespit edilmesi gerekir. Amaç fonksiyonu, ölçülen ve tahmin edilen hücre yığın gerilim noktaları arasındaki karesel hataların toplamı ile formüle edilmiştir. Seçilen bu amaç fonksiyonun temel amacı, tahmin edilen ve ölçülen I/V eğrileri arasında yeterli uyum sağlayarak yedi bilinmeyen parametreyi en iyi şekilde tahmin etmektir. Bahsedilen amaç fonksiyonu aşağıdaki gibi yazılabilir.

$$f(x_i) = \sum_{i=1}^{pl}(v_{meas}(i) - v_{est}(i))^2 \quad (8)$$

3. METOTLAR

Bu çalışmada PEMFC için optimal parametrelerin belirlenmesi amacıyla Zebra Optimizasyon Algoritması (ZOA) (Trojovska, Dehghani, & Trojovsky, 2022), Altın Çakal Optimizasyon algoritması (GJO) (Chopra & Ansari, 2022) ve Dhole Optimizasyon Algoritması (DOA) (Mohammed, Aghdasi, & Salehpour, 2025) seçilmiş ve kullanılmıştır.

3.1. Zebra Optimizasyon Algoritması

Zebra Optimizasyon Algoritması, 2022 yılında Trojovska ve diğerleri tarafından önerilmiş populasyon tabanlı bir optimizasyon algoritmasıdır (Trojovska vd., 2022). ZOA, doğada bulunan zebra sürülerinin otlanma ve avcıdan kaçma davranışlarından ilham alınarak geliştirilmiştir.

ZOA'da her bir zebra, aday çözüm olarak değerlendirilmektedir. ZOA temel olarak iki farklı fazdan oluşmaktadır: otlanma fazı ve avcıdan kaçma fazı (Trojovska vd., 2022). Otlama fazında, zebralar rastgele dağılmış durumdadır. ZOA'da en iyi popülasyon üyesi olan zebra öncü zebra olarak tanımlanmakta ve diğer populasyan üyelerini arama alanındaki konumuna doğru yönlendirmektedir (Trojovska vd., 2022). Bu

sayede aday çözümlerin geniş bir alanı taraması hedeflenmektedir. Avcıdan kaçma fazında ise zebraların yırtıcalara karşı savunma durumları dikkate alınmaktadır ve bu sayede pozisyonlarının güncellenmesi sağlanmaktadır (Trojovska vd., 2022). Bu fazda iki farklı olasılık durumu söz konusudur;

1) Zebralara aslanların saldırması: Zebralara aslanların saldırması durumunda, zebralar kendileri için farklı kaçış noktalarına doğru hareket ederler.
2) Zebralara diğer yırtıcıların saldırması: Diğer yırtıcılar popülasyon içindeki bir zebraya saldırdığında, diğer zebralar saldırıya uğrayan zebraya doğru hareket ederek bir savunma strateji gerçekleştirirler.

Böylece aday çözümlerin konumlarının iyileştirilmesi ve daha etkin çözümlerin elde edilmesi hedeflenmektedir.

Bulunan en iyi çözümler sonraki iterasyonlarda kullanılmak üzere hafızada saklanmakta ve sonraki iterasyon süreçlerinde kullanılmaktadır.

3.2. Altın Çakal Optimizasyon Algoritması

Altın Çakal Optimizasyon algoritması, Chopra ve Ansari tarafından 2022 yılında literatüre kazandırılmış popülasyon tabanlı bir optimizasyon algoritmasıdır (Chopra & Ansari, 2022). GJO, doğada buluna altın çakalların avı arama, kuşatma ve ava saldırma davranışlarından ilham alınarak geliştirilmiştir (Chopra & Ansari, 2022).

GJO'da, altın çakalların avlanma, avın enerjisinin azaltılması ve avın kuşatılarak saldırılması matemaktiksel olarak modellenmiştir. GJO'da altın çakallar, optimizasyon algoritması için aday çözüm olarak değerlendirilmekte ve av, ilgili problem için optimal çözüm olarak düşünülmektedir. Altın çakallar rastgele dağılarak, belirlenen arama uzayı içerisinde avı aramaktadırlar. Av, çakallar tarafından rahatsız edilerek,

enerjisinin azaltılması sağlanır (Chopra & Ansari, 2022). Daha sonraenerjisi azaltılan av, çakallar tarafından kuşatılarak yakalanmaktadır.Bu sayade, ele alınan problem için optimal çözüm bulunmaktadır.

3.3. Dhole Optimizasyon Algoritması

Dhole Optimizasyon Algoritması, Mohammed ve diğerleri tarafından 2025 yılında literatüre kazandırılmış populasyon tabanlı bir optimizasyon yöntemidir (Mohammed vd., 2025). DOA, dholelerin (bir tür yaban köpeği) avlanma stratejilerinden ilham alınarak geliştirilmiştir.

DOA'da, dholeler ilgili problem için olası aday çözümler ve av ilgili problem için optimal çözüm olarak değerlendirilmektedir. DOA, temel olarak üç fazdan oluşmaktadır (Mohammed vd., 2025). İlk faz olan arama fazında dholeler, belirlenen arama uzayı içerisine rastgele dağılmaktadırlar. Bu sayede arama uzayının tamamının aranması ve olası avların belirlenmesi sağlanmaktadır. İkinci faz olan çevreleme fazında, bir dhole tarafından belirlenen av, diğer popülasyon üyeleri tarafından çevrilir ve avın kaçmaması sağlanır. Bu sayede, aday çözümlerin optimal nokta etrafında yoğunlaşması sağlanmaktadır. Üçüncü faz ise saldırı fazı olarak adlandırılmaktadır. Bu fazda dholeler, ava doğru koordineli şekilde saldırarak avı yakalamaya çalışmaktadır. Bu sayade, ele alınan problem için optimal çözüm bulunmaktadır.

4. TEST DURUMLARI VE BULGULAR

Bu bölümde, iki farklı durum için PEMFC parametreleri, ZOA, GJO ve DOA yöntemleri ile belirlenmiştir. Gerçekleştirilen analizlerde popülasyon sayısı 150 ve iterasyon sayısı 100 olarak seçilmiştir.

4.1. BCS-500W PEMFC

Bu bölümde 500W gücüne ve 30A maksimum akıma sahip bir PEMFC için parametre analizleri gerçekleştirilmiştir. ZOA, GJO ve DOA ile elde edilen parametrelerle hesaplanan akım-gerilim değerleri, PEMFC için ölçülen akım-gerilim değerleri ile karşılaştırılmıştır. BCS-500W PEMFC ile ilgili detaylı bilgilere (Celtek, 2024), (Sun, Su, Yin, & Jermsittiparsert, 2020) ve (Kandidayeni, Macias, Khalatbarisoltani, Boulon, & Kelouwani, 2019) referanslarından ulaşılabilir.

ZOA, GJO ve DOA yöntemleri ile bulunan BCS-500 PEMFC parametreleri aşağıdaki tabloda verilmiştir.

Tablo 1. BCS-500W PEMFC için parametreler

	ξ_1	ξ_2 ($\times 10^{-3}$)	ξ_3 ($\times 10^{-5}$)	ξ_4 ($\times 10^{-5}$)	λ	R_c ($\times 10^{-3}$)	β
ZOA	-0.858	2.243	3.916	-18.763	18.860	0.323	0.014
GJO	-0.886	2.707	6.359	-18.954	20.807	0.338	0.015
DOA	-1.286	3.811	5.734	-19.302	21.955	0.135	0.017

BCS-500W PEMFC için elde edilen sonuçlar grafiksel olarak aşağıdaki şekilde gösterilmiştir.

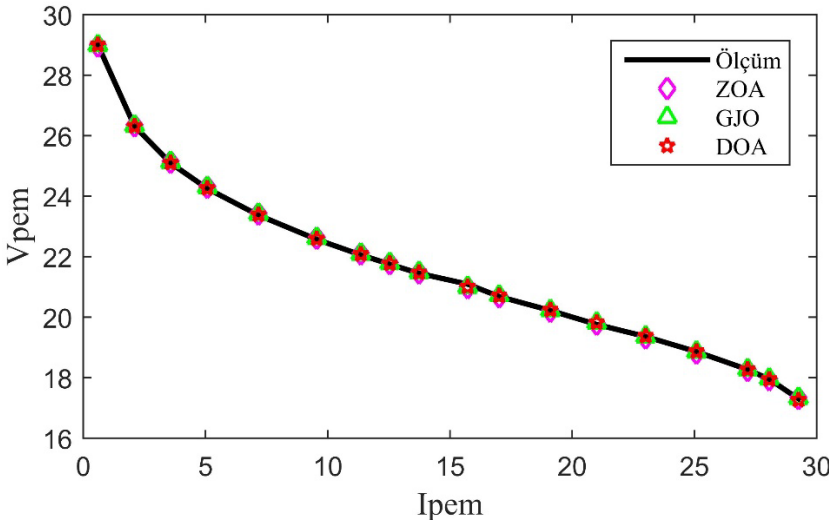

Şekil 1. BCS-500W için elde edilen grafikler

Burada elde edilen sonuçlar incelendiğinde, ZOA, GJO ve DOA ile bulunan grafikler, ölçüm grafiğine oldukça yakındır. Denklem 8'de verilen amaç fonksiyonu için; ZOA ile 0.0276 hata değeri, GJO ile 0.0220 hata değeri ve DOA ile 0.0186 hata değeri çıktıları oluşmuştur. Bu hata çıktıları dikkate alındığında, DOA ile bulunan grafik, GJO ve ZOA'ya kıyasla ölçüm değerlerine daha yakın olduğu söylenebilir.

4.2. Test Durumu 2: NedSStack PS6 PEMFC

Bu bölümde, 6kW NedSstack PEMFC için parametre analizleri gerçekleştirilmiştir. ZOA, GJO ve DOA ile elde edilen parametrelerle hesaplanan akım-gerilim değerleri, PEMFC için ölçülen akım-gerilim değerleri ile karşılaştırmalı olarak sunulmuştur. NedSstack PS6 PEMFC için detaylı bilgilere (Sun vd., 2020) ve (Kandidayeni vd., 2019) referanslarından ulaşılabilir.

ZOA, GJO ve DOA yöntemleri ile bulunan NedSStack PS6 PEMFC parametreleri aşağıdaki tabloda verilmiştir.

Tablo 2. NedSStack PS6 PEMFC için parametreler

	ξ_1	ξ_2 ($\times 10^{-3}$)	ξ_3 ($\times 10^{-5}$)	ξ_4 ($\times 10^{-5}$)	λ	R_c ($\times 10^{-3}$)	β
ZOA	-0.870	2.450	3.601	-9.540	13.000	0.133	0.021
GJO	-1.058	3.010	3.689	-9.540	13.039	0.104	0.057
DOA	-0.899	2.730	5.007	-9.540	13.000	0.100	0.058

NedSStack PS6 PEMFC için elde edilen sonuçlar grafiksel olarak aşağıdaki şekilde gösterilmiştir.

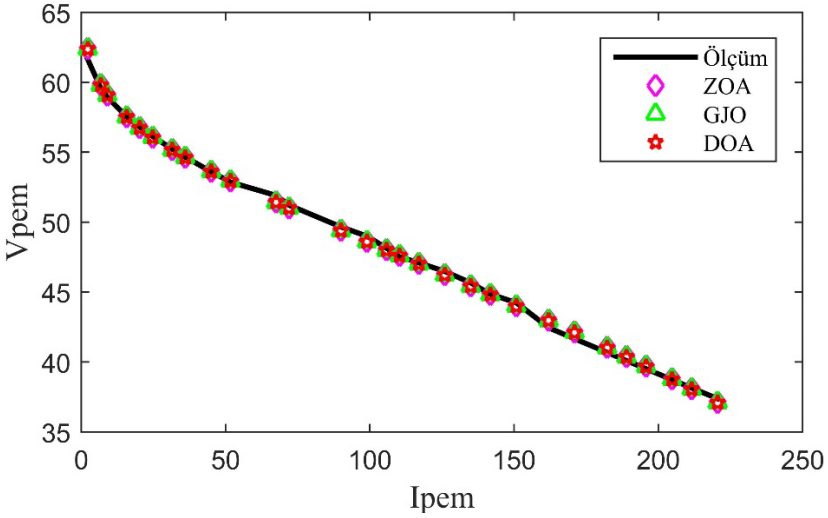

Şekil 2. NedSStack PS6 için elde edilen grafikler

Şekil 2'de verilen grafiklerde, ZOA, GJO ve DOA ile elde edilen grafiklerin, ölçüm grafiğine oldukça yakın olduğu açıkça görülmektedir. Denklem 8'de verilen amaç fonksiyonu için; ZOA ile 2.1941 hata değeri, GJO ile 2.1738 hata değeri ve DOA ile 2.1566 hata değeri çıktıları oluşmuştur. Bu hata çıktıları dikkate alındığında, DOA ile bulunan grafiğin, GJO ve ZOA'ya kıyasla ölçüm değerlerine daha yakın olduğu ifade edilebilir.

5. SONUÇ

PEMFC sistemlerinde parametre belirleme süreci, optimizasyon probleminin doğrusal olmayan, çok değişkenli ve çok modlu yapısından dolayı oldukça karmaşıktır ve çoğu zaman birden fazla yerel optimum çözüm içermektedir. Bu nedenle, geleneksel optimizasyon yöntemleri bu tür problemlerde yeterli tahmin hassasiyeti ve kararlılığı sağlamada zorlanmaktadır. Bu kapsamda Zebra Optimizasyon Algoritması, Altın Çakal Optimizasyon algoritması ve Dhole Optimizasyon Algoritması yöntemleri, proton değişim membranlı yakıt hücrelerinin

parametrelerinin belirlenmesi amacıyla kullanılmıştır. BCS-500W ve NedSstack PS6 proton değişim membranlı yakıt hücreleri için, yedi farklı parametre değerleri bu yöntemler aracılığıyla elde edilmiştir. Bu PEMFC'ler için bulunan değerler, grafiksel olarak ölçüm değerleri ile karşılaştırmalı olarak sunulmuştur. Ayrıca, ölçüm değerleri ile belirtilen yöntemler aracılığıyla bulunan değerler arasındaki hata çıktıları da sayısal olarak verilmiştir. Elde edilen sonuçlardan, DOA yöntemi ile diğer iki yönteme göre daha düşük hata çıktı değerleri elde edildiği gözlemlenmiştir. Bu nedenle, hem BCS-500W hem de NedSstack PS6 PS6 proton değişim membranlı yakıt hücrelerinin parametrelerinin belirlenmesinde, DOA yönteminin daha başarılı olduğu gözlemlenmiştir.

KAYNAKÇA

Ayyarao, Tummala. S. L. V., Polumahanthi, N., & Khan, B. (2024). An accurate parameter estimation of PEM fuel cell using war strategy optimization. Energy, 290, 130235. doi:10.1016/j.energy.2024.130235

Celtek, S. A. (2024). Estimation of PEMFC design parameters with social learning-based optimization. Electrical Engineering, 106(4), 4457-4468. doi:10.1007/s00202-023-02221-7

Chopra, N., & Ansari, M. M. (2022). Golden jackal optimization: A novel nature-inspired optimizer for engineering applications. Expert Systems with Applications, 198. doi:10.1016/j.eswa.2022.116924

El-Fergany, A. A. (2018). Extracting optimal parameters of PEM fuel cells using SALP swarm optimizer. Renewable Energy, 119, 641–648. doi:10.1016/j.renene.2017.12.051

Hachana, O., & El-Fergany, A. A. (2022). Efficient PEM fuel cells parameters identification using hybrid artificial bee colony Differential Evolution Optimizer. Energy, 250, 123830. doi:10.1016/j.energy.2022.123830

Kandidayeni, M., Macias, A., Khalatbarisoltani, A., Boulon, L., & Kelouwani, S. (2019). Benchmark of proton exchange membrane fuel cell parameters extraction with metaheuristic optimization algorithms. Energy, 183, 912-925. doi:10.1016/j.energy.2019.06.152

Mbasso, W. F., Hussein Farh, H. M., Harrison, A., & Al-Shamma'a, A. A. (2025). Hybrid metaheuristic optimization for proton exchange membrane fuel cell parameter estimation in Hydrogen Energy Systems. International Journal of Hydrogen Energy, 160, 150505. doi:10.1016/j.ijhydene.2025.150505

Mohammed, B. O., Aghdasi, H. S., & Salehpour, P. (2025). Dhole optimization algorithm: a new metaheuristic algorithm for solving optimization problems. Cluster Computing, 28(7). doi:10.1007/s10586-024-05005-1

Menesy, A. S., Kotb, K. M., Sultan, H. M., Bukar, A. L., Ramadan, H. A., Kassas, M., … Kamel, S. (2025). Parameter estimation and sensitivity analysis of proton exchange membrane fuel cells based on electric eel foraging optimization algorithm. International Journal of Hydrogen Energy, 153, 150100. doi:10.1016/j.ijhydene.2025.150100

Rezk, H., Ferahtia, S., Djeroui, A., Chouder, A., Houari, A., Machmoum, M., & Abdelkareem, M. A. (2022). Optimal parameter estimation strategy of PEM fuel cell using gradient-based optimizer. Energy, 239, 122096. doi:10.1016/j.energy.2021.122096

Sun, S., Su, Y., Yin, C., & Jermsittiparsert, K. (2020). Optimal parameters estimation of PEMFCs model using Converged Moth Search Algorithm. Energy Reports, 6, 1501-1509. doi:10.1016/j.egyr.2020.06.002

Trojovska, E., Dehghani, M., & Trojovsky, P. (2022). Zebra Optimization Algorithm: A New Bio-Inspired Optimization Algorithm for Solving Optimization Algorithm. IEEE Access, 10, 49445-49473. doi:10.1109/access.2022.3172789

Xu, S., Wang, Y., & Wang, Z. (2019). Parameter estimation of proton exchange membrane fuel cells using eagle strategy based on Jaya algorithm and Nelder-Mead Simplex Method. Energy, 173, 457–467. doi:10.1016/j.energy.2019.02.106

RECENT ADVANCES IN PHOTOVOLTAIC (PV) TECHNOLOGIES: ENERGY EFFICIENCY TRENDS AND SOLAR TRACKING INNOVATIONS

Tugba GURLER[1]

Safiullah SHIRZAD[2]

1. INTRODUCTION

Solar energy is the main source of energy. Furthermore, it's the oldest types of energy ever used by humans and ancient civilizations believed that sun is a powerful god. Drying foods through solar energy is known the first application of solar energy (Kalogirou, 2004 as cited in Kalogirou 2009) The earliest known large-scale application of solar energy is likely the legendary burning of the Roman fleet in Syracuse by the Greek mathematician and philosopher Archimedes around 212 B.C. For over a thousand years, from 100 B.C. to 1100 A.D., this event was frequently cited by various authors. However, it was later dismissed by some as a myth, with skeptics arguing that the technology to create the necessary mirrors did not exist at the time (Delyannis, 1967 as cited in Kalogirou 2009). The central debate revolved around whether Archimedes possessed sufficient knowledge of optics to concentrate on sunlight and set fire to ships from a distance. It is known that he authored a treatise titled *On Burning Mirrors* (Meinel and Meinel, 1976), though the original text has been lost and is only known through references.

[1] Assistant Prof, Hitit Universuty, Faculty of Engineering and Natural Sciences, Departmant of Mechanical Engineering, ORCID: 0000-0003-3255-5521.

[2] Graduate, Hitit University, Institute of Graduate Studies Department of Interdisciplinary Energy Systems Engineering, ORCID: 0009-0000-8724-0418

The event was recorded by the Greek historian Plutarch (46–120 A.D.), who noted that the Romans thought they were fighting supernatural forces after seeing unexplained devastation. The incident was later described in detail by the Polish mathematician Vitelio in his work *Optics*, which described "the burning glass of Archimedes composed of 24 mirrors, which conveyed the rays of the sun into a common focus and produced an extra degree of heat" (Delyannis and Belessiotis, 2000; Delyannis, 1967 as cited in Kalogirou 2009).

Centuries later, during the Byzantine era, the scholar Proclus reportedly replicated Archimedes' experiment, successfully burning the fleet of enemies besieging Constantinople (Delyannis, 1967). In the 17th century, Athanasius Kircher (1601–1680) attempted to test the legend's scientific validity by trying to ignite a woodpile at a distance. Unfortunately, no records of his findings have survived (Meinel and Meinel, 1976 as cited in Kalogirou 2009).

According to a widely accepted alternate opinion among historians, Archimedes used soldiers' polished shields rather than polished mirrors. The sun's beams could have been focused onto a single location on an enemy ship by arranging these shields to create a massive parabolic reflector. Whether true or not, this tale provided an early illustration of the enormous power found in sun radiation.

Remarkably, the earliest documented attempts to harness solar energy involved the use of concentrating collectors. These systems are inherently complex, requiring precise construction and the ability to track the sun. During the 18th century, solar furnaces capable of melting metals like iron and copper were constructed across Europe and the Middle East using materials such as polished iron, glass lenses, and mirrors. A notable example was built around 1774 by the renowned French chemist

Antoine Lavoisier. He used a powerful lens system—a primary lens of 1.32 meters paired with a secondary 0.2-meter lens—to concentrate sunlight and achieve an extraordinary temperature of 1750°C, a record that stood for a century (see Figure 1). Around the same time, the French naturalist Georges-Louis Leclerc, Comte de Buffon (1747–1748) (Kalogirou, S. (2009), and Delyannis, 2003 conducted experiments with what he termed "hot mirrors burning at long distance as cited in Kalogirou 2009.

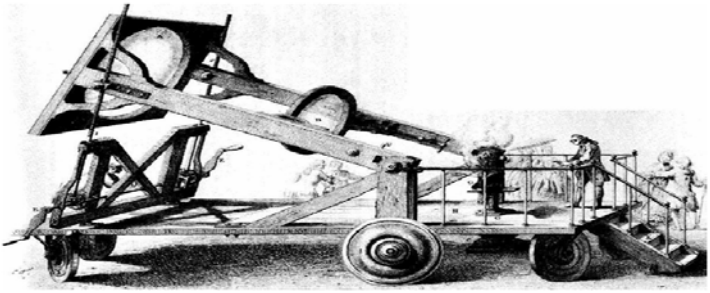

Figure 1. (1774), Lavoisier's solar furnace (Kalogirou, S. 2009)

2. TECHNOLOGICAL DEVELOPMENTS IN PV SYSTEMS AND THEIR PERFORMANCE METRICS

Photovoltaic (PV) efficiency is a key metric for assessing the performance of solar cells and modules. It indicates how effectively a photovoltaic device transforms incoming solar energy into usable electrical power. Improved conversion efficiency enables a solar module to produce more electricity from the same area, which is especially crucial in situations where space for installation is restricted, such as in residential rooftop systems and urban settings. The ratio of the power output produced to the solar power received by the cell's surface is known as the efficiency of a solar cell. This can be expressed numerically as

$$\eta = \frac{Pout}{Pin} \times 100 \quad (1)$$

where ηis the conversion efficiency, P_outis the electrical power produced by the solar cell, and P_inis the solar irradiance incident on the cell surface. Under standard test conditions (STC), the incident solar irradiance is typically assumed to be 1000 W/m², with a cell temperature of 25°C and an air mass (AM) value of 1.5.

The material utilized, the structure of the cells, the manufacturing process, and the operating environment all affect how efficient photovoltaic systems are. For commercial products, the module efficiencies of traditional crystalline silicon technologies, which dominate the global PV market, usually range from 18% to 23%. Because of its more homogeneous crystal structure and lower electron recombination losses, monocrystalline silicon cells often have higher efficiencies than polycrystalline ones. High-efficiency technologies like passivated emitter and rear cell (PERC), heterojunction (HJT), and interdigitated back contact (IBC) solar cells have been developed as a result of recent developments in silicon cell architecture.

Emerging solar materials have shown encouraging efficiency gains over traditional silicon-based technology. In addition to providing benefits like lightweight construction and flexible applications, thin-film technologies, such as copper indium gallium selenide (CIGS) and cadmium telluride (CdTe), often attain commercial efficiencies in the region of 14–20%. Perovskite solar cells have garnered a lot of scientific interest lately because of their quick efficiency gains, which have allowed them to achieve laboratory efficiencies of 25% in a comparatively short amount of time (NREL, n.d).

Furthermore, tandem photovoltaic technologies, particularly perovskite–silicon tandem cells, have demonstrated efficiencies exceeding 30% in laboratory conditions by combining multiple semiconductor layers to capture a wider portion of the solar spectrum (NREL, n.d).

It is important to note that laboratory efficiencies are often higher than commercially available module efficiencies due to ideal testing conditions and smaller cell sizes. In real-world operating conditions, several factors can influence the effective efficiency of PV systems. Factors influencing photovoltaic system performance encompass temperature variations, shading, dust buildup, module deterioration, inverter inefficiencies, and system configuration aspects like tilt and orientation. Furthermore, environmental elements such as fluctuating solar radiation and ambient temperature can substantially impact overall system output.

Current research and development initiatives are focused on boosting PV efficiency through the use of advanced materials, refined cell designs, and sophisticated system optimization methods. Table 1 shows the typical efficiency of the different solar cells (NREL, 2026).

Table 1. Typical PVs efficiencies

PV Technology	Typical Commercial Efficiency
Monocrystalline Silicon	20–23%
Polycrystalline Silicon	17–20%
PERC	21–23%
HJT	22–25%
CdTe Thin Film	16–19%
CIGS Thin Film	15–20%
Perovskite (lab)	25–26%
Perovskite–Silicon Tandem (lab)	30–33%

(NREL, 2026)

These advancements not only increase energy generation but also lower the levelized cost of electricity derived from solar

energy, thereby enhancing the competitiveness of photovoltaic technology against traditional energy sources figure 2, figure 3 and , figure 4, figure 5 shows the efficiency of the crystalline and perovskite solar panels(Viridian Solar, n.d.; NREL, n.d.)

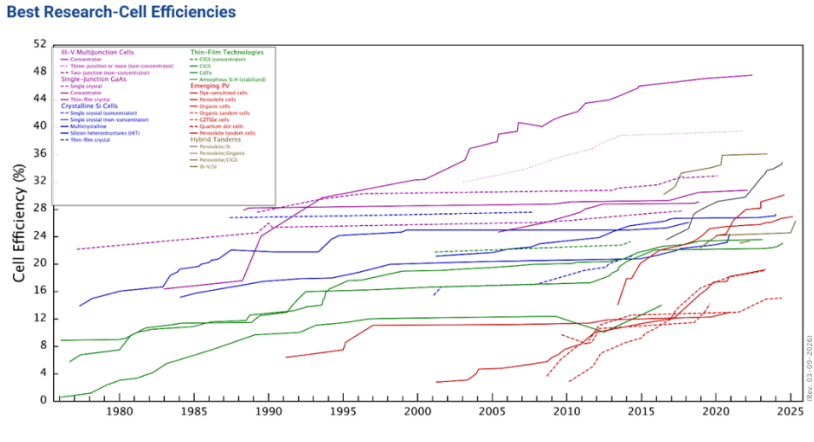

Figure 2. Historical Progress of Best Research Cell Efficiencies for Different Photovoltaic Technologies (NREL, 2026), Interactive Best Research-Cell Efficiency Chart | Photovoltaic Research | NLR

figure 7 illustrates the historical development of the best research cell efficiencies for various photovoltaic (PV) technologies over several decades. The graph presents the evolution of solar cell performance from the mid-1970s to recent years, highlighting the improvements achieved through technological advancements and material innovations (NREL, n.d) . The vertical axis represents the cell efficiency (%), while the horizontal axis represents the year of development. Different colored lines correspond to different photovoltaic technologies, including multijunction cells, single-junction gallium arsenide (GaAs), crystalline silicon cells, thin-film technologies (such as CdTe and CIGS), and emerging photovoltaic technologies like perovskite and dye-sensitized solar cells.

From the figure, it can be observed that multijunction cells exhibit the highest efficiencies, reaching values above 45% under concentrated sunlight conditions. Crystalline silicon cells, which dominate the commercial PV market, show steady improvement and currently achieve efficiencies close to 27–28% in laboratory conditions. Thin-film technologies demonstrate moderate efficiencies but offer advantages in terms of lower material consumption and flexible applications. Emerging technologies such as perovskite solar cells have shown rapid efficiency growth in a relatively short time period, indicating strong potential for future photovoltaic applications.

Overall, the figure demonstrates the continuous progress in photovoltaic research driven by advancements in semiconductor materials, device architectures, and fabrication techniques. Figure 8 presents a detailed version of the National Renewable Energy Laboratory (NREL) Best Research-Cell Efficiency Chart, which provides verified record efficiencies achieved by different photovoltaic technologies worldwide. In contrast to the simplified representation in Figure 2, this chart includes individual research institutions, laboratories, and companies responsible for the record efficiencies.

Each marker on the graph corresponds to a verified experimental result reported by organizations such as NREL, Fraunhofer ISE, Stanford University, Sharp, Panasonic, and other research institutions. The figure also categorizes photovoltaic technologies into several groups, including:

- III–V multijunction solar cells
- Single-junction GaAs cells
- Crystalline silicon solar cells
- Thin-film technologies (CIGS, CdTe, amorphous silicon)

- Emerging photovoltaic technologies such as perovskite, organic, and quantum-dot cells
- Hybrid tandem technologies (e.g., perovskite-silicon tandems)

The chart demonstrates that III–V multijunction solar cells achieve the highest laboratory efficiencies, approaching 48% under concentrated illumination. Meanwhile, perovskite-silicon tandem cells have recently surpassed 30% efficiency, representing a major breakthrough in next-generation photovoltaic technology. The figure highlights the significant role of international research collaborations and advanced materials engineering in improving solar cell performance.

Figure 3, figure 4 and figure 5 focus specifically on the efficiency progress of crystalline silicon solar cells, which represent the most widely used photovoltaic technology in the global solar market (NREL, n.d).

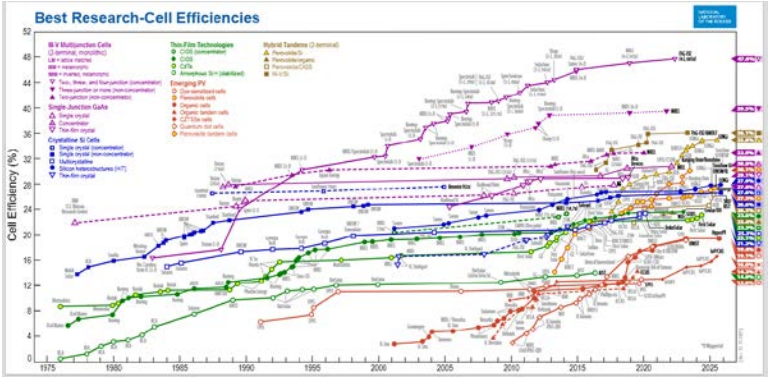

Figure 3. Detailed National Renewable Energy Laboratory (NREL) Chart of Record Photovoltaic Cell Efficiencies (NREL, n.d.)), Best Research-Cell Efficiency Chart | Photovoltaic Research | NLR

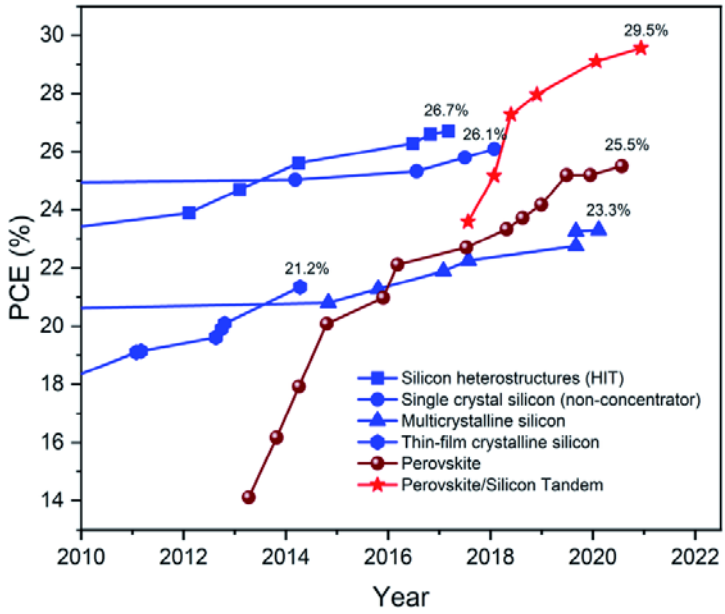

Figure 4. efficiency of crystalline solar cells (Shrivastav et al, 2021)

The highlighted section of the chart emphasizes the development of different silicon-based cell structures over time.

The main categories shown include: Single-crystal silicon cells;; Multicrystalline silicon cells (mSi); Silicon heterojunction (HIT/HJT) cells; Thin-film crystalline silicon cells and Concentrator silicon cells.

Over the past four decades, the efficiency of crystalline silicon solar cells has steadily increased due to improvements in cell architecture, surface passivation, light-trapping techniques, and advanced manufacturing processes. Early silicon solar cells in the 1970s exhibited efficiencies around 14–16%, whereas modern laboratory silicon cells now exceed 27% efficiency.

The figure highlights the remarkable technological progress achieved through innovations such as passivated emitter and rear cell (PERC) technology, heterojunction structures, and

advanced contact designs. These advancements have allowed crystalline silicon technology to maintain its dominance in the photovoltaic market due to its high reliability, mature manufacturing processes, and continuously improving efficiency.

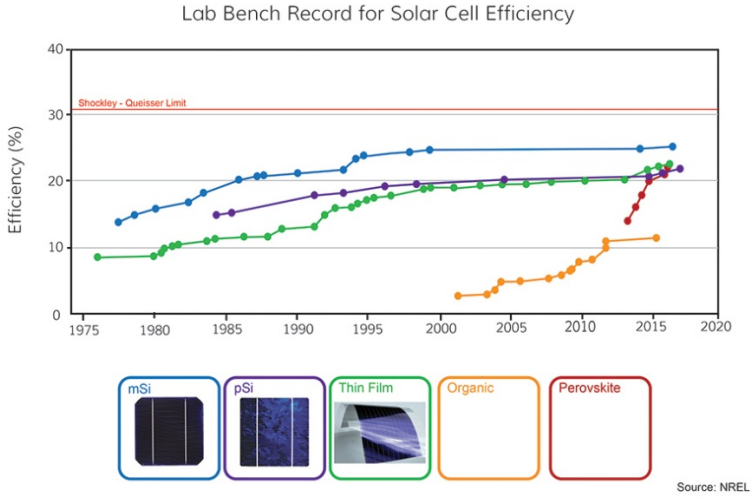

Figure 5 Solar cell efficiency (Viridian Solar, n.d.; NREL, n.d.)

3. CURRENT SOLAR TRACKING SYSTEMS

Solar photovoltaic (PV) systems can be installed in various configurations depending on energy demand, geographical location, and system efficiency requirements. One important method for improving the energy output of PV systems is the use of solar tracking systems. A solar tracking system is a mechanism that continuously adjusts the orientation of photovoltaic panels to follow the apparent movement of the sun across the sky during the day. By maintaining the solar panels closer to the normal incidence of solar radiation, tracking systems increase the amount of solar irradiance captured by the PV modules and consequently improve electricity generation.

Solar tracking systems are generally classified into two main categories: single-axis tracking systems and dual-axis tracking systems (See in Figure 4).

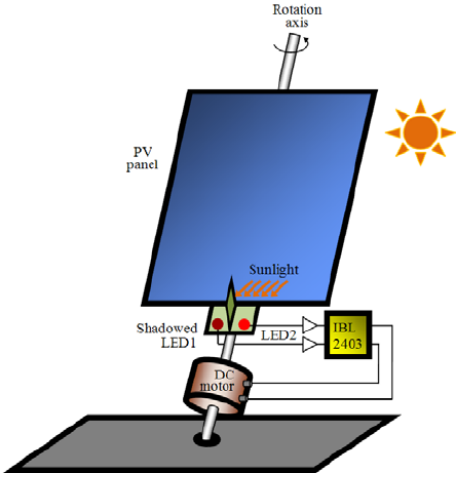

Figure 4. Conceptual diagram of a single-axis solar tracking system. (Tudorache et al., 2012)

A single axis tracking system rotates the solar panel around a single rotational axis, typically following the sun's path from east to west. In some configurations, the axis may be aligned north–south, allowing the panel to tilt east–west throughout the day. This design enables the PV panel to track the daily movement of the sun but does not fully compensate for seasonal variations in solar elevation.

In contrast, a dual-axis tracking system allows movement along two perpendicular axes, commonly referred to as the azimuth axis (east–west) and the elevation axis (north–south). This configuration enables the photovoltaic panel to follow the sun's position more accurately throughout both the daily and seasonal cycles. By continuously adjusting its orientation in two directions, the panel can maintain a position that is nearly perpendicular to incoming solar radiation, thereby maximizing the received solar energy. The below Figure 5 and Figure 6

,presents the solar tracking-axis angles, mechanical structure of the dual axis solar tracking systems and dual axis tracker block diagram respectivel

Figure 5. solar tracking angles and mechanical structure of the dual-axis solar tracking system (Hammas et al., 2025)

Figure 6. below explains,a block diagram of a control system, specifically designed for a two-axis (Azimuth and Tilt) position control system, likely for something like a radar, antenna, solar panel, or a robotic arm.

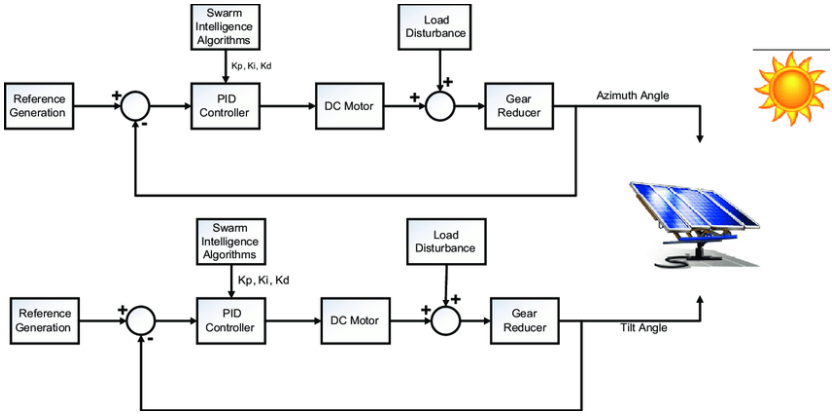

Figure 6. Dual axis-sun tracker block diagram (Sabir et al., 2016)

The diagram shows two identical control loops running in parallel—one for the Azimuth Angle (horizontal rotation) and one for the Tilt Angle (vertical rotation).

Here is a breakdown of the components and the flow of the diagram:

1. The Controller Optimization Stage (Top Left: "Reference Generation")

Swarm Intelligence Algorithms: This box represents the "brains" of the design phase. Instead of a human tuning the controller, an algorithm (like Particle Swarm Optimization or Ant Colony Optimization) is used.

K_p,K_i,K_d: These are the proportional, integral, and derivative gains for a PID controller. The "Swarm Intelligence" box is responsible for automatically calculating the optimal values for these three parameters to achieve the best system performance.

2. The Control Loop (Per Axis)

The diagram then splits into two identical paths: one for the Azimuth axis and one for the Tilt axis. Each path functions the same way:

Input (Reference Generation) system is given a desired position (a target Azimuth or Tilt angle). Summation Node (The Circle) compares the desired position (input) with the current position (feedback). It calculates the error (the difference between where it should be and where it is). PID Controller uses the K_p,K_i,K_d values provided by the Swarm Algorithm, this controller calculates the appropriate power or command needed to fix the error. DC Motor is the actuator that physically moves the axis. Gear Reducer is connected to the motor. It reduces the high speed of the motor while increasing the torque (rotational force) to move the heavy load smoothly and precisely. Load

Disturbance arrow represents external forces trying to disrupt the system's position. For example, wind pushing against a radar dish or an antenna, or imbalance in the load. The system must resist these disturbances. Output (Azimuth Angle / Tilt Angle) is the final physical position of the system.

3. The Feedback Loop

The actual output angle (Azimuth or Tilt) is measured and fed back to the summation node at the beginning. This closes the loop, allowing the system to continuously monitor and correct its position.

Several studies have demonstrated that solar tracking systems can significantly enhance the performance of photovoltaic installations. In particular, dual-axis tracking systems are generally considered the most effective in terms of energy gain because they maintain optimal alignment between the PV module surface and the direction of solar radiation throughout the day. Research indicates that dual-axis tracking systems can increase energy output by approximately 25–45% compared to fixed PV installations, depending on geographical location and system design (Hammas et al., 2025). Consequently, dual-axis trackers are widely investigated for applications where maximizing energy production is a priority. However, despite their higher energy yield, dual-axis systems are typically more complex and expensive than single-axis trackers due to additional mechanical components, control systems, and maintenance requirements. Therefore, the selection of an appropriate tracking configuration often involves a trade-off between energy efficiency, system complexity, installation cost, and maintenance considerations.

Regional case studies further support these conclusions. A six-month comparative study in northern Lebanon showed that dual-axis tracking systems captured 38% more energy than fixed

systems (Atallah et al., 2025).In addition, comparative analyses of polycrystalline and monocrystalline panels under tracking conditions revealed that polycrystalline panels performed more efficiently within tracking systems (Akpinar et al., 2025),emphasizing the importance of appropriate module selection alongside tracking design.

However, not all studies conclude that tracking is universally superior. A 100 kWp rooftop system in Tururo city, UK, analyzed using PVsyst and real-time meteorological data, found that a fixed system at zero-degree azimuth achieved the highest energy yield without requiring tracking and improved simulation accuracy by 9% compared to similar studies (Hosseini et al., 2025). This suggests that optimal configuration depends strongly on local climatic and design conditions. Similarly, research on a 2 MWp floating solar system simulated with PVsyst demonstrated that while dual-axis tracking achieved the highest efficiency and lowest losses compared to fixed, seasonal, and single-axis systems, installation type and system configuration significantly influenced overall performance outcomes (Avasthi et al., 2025).

Although substantial research confirms the energy advantages of tracking systems, variations in climatic conditions, installation types, and module technologies indicate the necessity of location-specific evaluation. Therefore, further investigation integrating accurate meteorological data, optimized PV module selection, and detailed simulation under tracking configurations remains essential to determine the most efficient system design for specific regional applications.The Net Present Value (NPV) represents the difference between the present value of the project's revenues and the present value of its costs over the system lifetime. A positive NPV indicates that the project is economically feasible.

4. CONCLUSION

This chapter has provided a comprehensive overview of advanced photovoltaic technologies. The analysis of PV types demonstrated that while monocrystalline and polycrystalline silicon continue to dominate the commercial market with efficiencies of 20–23% and 17–20% respectively, significant research efforts are directed toward next-generation technologies. Among these, all-perovskite tandem solar cells have emerged as a particularly promising approach, achieving certified power conversion efficiencies exceeding 30% in two-terminal configurations. The ability to precisely tune perovskite bandgaps enables optimal spectral utilization through monolithic stacking of wide-bandgap (≈1.8 eV) and narrow-bandgap (≈1.2 eV) sub cells, connected by efficient tunnel recombination junctions. This architecture substantially reduces thermalization losses, enabling performance beyond the fundamental limits of single-junction devices. The rapid efficiency progression documented in this chapter, from initial demonstrations to current record cells exceeding 30%, underscores the tremendous potential of this technology for future commercial deployment.

Solar tracking systems were examined as a key strategy for improving PV system performance. The comparative analysis of single-axis and dual-axis tracking configurations highlighted the trade-offs between energy yield and system complexity. Dual-axis trackers, which maintain near-perpendicular alignment with solar radiation throughout daily and seasonal cycles, can increase energy output by approximately 25–45% compared to fixed installations. However, their additional mechanical components and control requirements necessitate careful economic evaluation for specific applications.

Looking forward, the continued decline in solar PV costs—86% reduction in installed costs since 2010 according to

IRENA data—combined with emerging technologies such as floating PV, building-integrated photovoltaics, and perovskite-based tandems, positions solar energy as a cornerstone of global sustainable energy systems. The integration of intelligent control systems, data-driven optimization techniques, and appropriate policy frameworks will be essential for realizing this potential. As global solar PV costs continue to decline and technologies advance, the lessons from both high-efficiency laboratory research and real-world deployment in challenging environments provide valuable guidance for accelerating the transition toward sustainable, affordable, and reliable solar energy worldwide.

REFERENCES

Atallah, J., Rahme, P., & Issa, J. S. (2025). Comparative assessment of single axis manual solar PV trackers: A case study for agricultural applications. Energy Conversion and Management: X, 26, 100927.

Akpinar, E., Katircioglu, G. G., & Das, M. (2025). Effects of solar tracking on different types of solar panels; experimental study for thermal and photovoltaic types. International Journal of Hydrogen Energy, 144, 611-620.

Avasthi, A., Garg, R., & Mahajan, P. (2025). Optimizing energy harvesting: a comprehensive analysis of tracking technologies in a 2 MW P floating solar photovoltaic system. Electrical Engineering, 107(4), 4663-4681.

Delyannis, E. (1967). Historical background of desalination and renewable energy. Solar Energy, 10(3), 95–102.

Delyannis, E. (2003). Historic background of desalination and renewable energy. Solar Energy, 75(5), 357–366.

Delyannis, E., & Belessiotis, V. (2000). Solar desalination: A historical review. Desalination, 128(1), 63–72.

Hammas, M., Fituri, H., Shour, A., Khan, A. A., Khan, U. A., & Ahmed, S. (2025). A Hybrid Dual-Axis Solar Tracking System: Combining Light-Sensing and Time-Based GPS for Optimal Energy Efficiency. *Energies*, *18*(1), 217. https://doi.org/10.3390/en18010217

Hosseini, S. A., Mansoori Al-yasin, S. A., Gheibi, M., & Moezzi, R. (2025). Evaluation of Solar Energy Performance in Green Buildings Using PVsyst: Focus on Panel Orientation and Efficiency. Eng, 6(7), 137.

Kalogirou, S. A. (2004). Solar thermal collectors and applications. Progress in Energy and Combustion Science, 30(3), 231–295. https://doi.org/10.1016/j.pecs.2004.02.001

Kalogirou, S. (2009). Solar energy engineering: Processes and systems. Academic Press.

Meinel, A. B., & Meinel, M. P. (1976). Applied solar energy: An introduction. Addison-Wesley.

National Renewable Energy Laboratory. (NREL). https://www.nrel.gov/analysis/renewable-electricity.htmlBest Research-Cell Efficiency Chart | Photovoltaic Research | NLR (Accessed online 09/03/2026)

Sabir, M. M., & Ali, T. (2016). Optimal PID controller design through swarm intelligence algorithms for sun tracking system. *Applied Mathematics and Computation*, *274*, 690-699.

Shrivastav, N., Madan, J., Pandey, R., & Shalan, A. E. (2021). Investigations aimed at producing 33% efficient perovskite–silicon tandem solar cells through device simulations. RSC advances, 11(59), 37366-37374.

Tudorache, T., Oancea, C., & Kreindler, L. (2012). Performance evaluation of a solar tracking PV panel. Procedia Engineering, 69, 1201–1208.

Viridian Solar. (n.d.). *Resources: 4.2.1 solar cell efficiencies*. Retrieved March 8, 2026, from https://www.viridiansolar.co.uk/resources-4-2-1-solar-cell-efficiencies.html?utm_source

GRADYAN KIRILMA İNDİSLİ LENS ANTENLER: TEMEL İLKELER, YAPISAL TÜRLER, PERFORMANS ÖLÇÜTLERİ VE MODERN HABERLEŞME UYGULAMALARI

Burak DÖKMETAŞ[1]

1. GİRİŞ

Kablosuz haberleşme sistemlerinde artan veri iletim hızları, kullanıcı yoğunluğu ve daha yüksek frekans bantlarına yönelim, anten tasarımında yeni gereksinimleri beraberinde getirmiştir (Arican ve ark.,2019; Dokmetas ve ark.,2019). Günümüzde antenlerden yalnızca düşük maliyet ve enerji verimliliği değil; aynı zamanda geniş bantlı çalışma, düşük kayıp, düşük yan lob seviyesi ve ışınım örüntüsünün etkin biçimde kontrol edilebilmesi beklenmektedir. Özellikle milimetre dalga uygulamalarında serbest uzay yol kayıplarının artması, yüksek yönlülüğe sahip anten çözümlerini daha önemli hâle getirmiştir (Dokmetas ve ark.,2023; Dokmetas ve ark.,2024). Bu bağlamda lens antenler, yüksek kazanç ve yönlendirilmiş ışınım sağlayabilmeleri nedeniyle radar, uydu haberleşmesi ve yüksek veri hızlı kablosuz bağlantılar gibi alanlarda dikkat çekici bir alternatif oluşturmuştur. Bazı uygulamalarda lens antenler, daha karmaşık ve maliyetli faz dizi antenlerin yerine de kullanılabilmektedir.

Lens antenler genel olarak bir dielektrik lens gövdesi ve onu aydınlatan bir besleme anteninden oluşur. Dielektrik lens antenlerin önemli avantajlarından biri geniş bantlı olmalarıdır;

[1] Dr. Öğr. Üyesi, Kafkas Üniversitesi, Mühendislik Fakültesi, Elektrik-Elektronik Mühendisliği Bölümü, ORCID: 0000-0001-5900-6691.

çoğu durumda çalışma frekans aralığı lens gövdesinden çok besleme anteninin bant genişliği ile sınırlanır. Dielektrik lens antenler temel olarak homojen ve homojen olmayan olmak üzere iki ana sınıfta değerlendirilebilir. Homojen lenslerde ışınım örüntüsünün kontrolü büyük ölçüde lens geometrisi ile sağlanırken, homojen olmayan yapılarda dalga cephesinin dönüşümü lens profili boyunca değişen kırılma indisi dağılımı ile gerçekleştirilir. Bu ikinci grup, gradyan kırılma indisli ya da kısaca GRIN lens antenler olarak adlandırılmaktadır.

GRIN lens antenlerde ışınım özellikleri yalnızca lensin şekline ve boyutlarına değil, aynı zamanda kırılma indisinin uzaysal dağılımına da bağlıdır. Bu durum tasarımcıya ek bir elektromanyetik serbestlik sunarak yüksek yönlülük, düşük yan lob seviyesi ve geniş açılı tarama gibi avantajların aynı yapıda bir araya getirilmesine olanak tanır. Bu nedenle GRIN lensler, çok ışınlı çalışma ve pasif ışın yönlendirme gerektiren sistemlerde önemli bir çözüm hâline gelmiştir. Bununla birlikte, istenen indis dağılımının pratikte elde edilmesi uzun süre bu yapıların yaygın kullanımını sınırlayan temel zorluklardan biri olmuştur.

GRIN lenslerin gerçekleştirilmesinde geçmişte çok katmanlı dielektrik yapılar, delikli katı dielektrikler ve metal tabanlı periyodik yapılar kullanılmıştır. Ancak bu yöntemler çoğu zaman yüksek üretim hassasiyeti, karmaşık montaj süreçleri ve uzun imalat süreleri gerektirmiştir. Son yıllarda eklemeli imalat teknolojilerinin gelişmesi, karmaşık gradyan indis dağılımlarının daha kısa sürede ve daha düşük maliyetle üretilebilmesini mümkün kılmıştır. Özellikle FDM, SLA, jet modeling ve seçici lazer sinterleme gibi yöntemler, mikrodalga bantlardan sub-THz ve THz bölgesine kadar uzanan geniş bir frekans aralığında GRIN lens anten tasarımlarının uygulanabilirliğini artırmıştır. Böylece yalnızca klasik lens geometrileri değil, aynı zamanda düzleştirilmiş, dönüştürülmüş ve uygulamaya özel optimize edilmiş lens yapıları da daha erişilebilir hâle gelmiştir.

GRIN lens ailesi içinde Luneburg, Fresnel, Mikaelian ve Eaton gibi farklı lens tipleri öne çıkmaktadır. Bunlar arasında özellikle Luneburg lensler, yüksek yönlülük, geniş açılı tarama ve çoklu besleme ile çok ışın üretimi gibi özellikleri nedeniyle literatürde geniş yer bulmaktadır. Bununla birlikte, Luneburg yapılarının daha geniş GRIN lens yaklaşımı içinde değerlendirilmesi, konunun hem teorik hem de uygulamalı yönlerinin daha bütüncül biçimde ele alınmasını sağlamaktadır. Bu bölümde gradyan kırılma indisli lens anten yapıları; temel prensipleri, başlıca tasarım yaklaşımları ve modern uygulama alanları çerçevesinde derleme niteliğinde incelenecektir.

2. GRIN LENS ANTENLERİN TEMELLERİ

2.1. Lens Anten Kavramı ve GRIN Yaklaşımı

Gradient index (GRIN) lens yapıları, elektromanyetik dalgaların fazını ve yayılım yönünü kontrol ederek anten sistemlerinde kazanç artışı, ışın daraltma ve alan dağılımının iyileştirilmesi gibi önemli avantajlar sunmaktadır. Son yıllarda bu lenslerin 3B baskı teknikleriyle üretilmesi, hem maliyet hem de üretim esnekliği açısından dikkat çekici bir araştırma alanı hâline gelmiştir. Literatürde, GRIN lenslerin temel çalışma prensibinin, farklı radyal bölgelerde farklı etkin dielektrik sabitleri oluşturarak gelen küresel dalga cephesini düzlemsel hâle dönüştürmek olduğu vurgulanmaktadır. Bu amaçla, baskı sırasında tek bir dielektrik malzemenin doluluk oranı değiştirilerek farklı etkin kırılma indisleri elde edilebilmektedir. Böylece klasik çok parçalı ya da karmaşık üretim gerektiren lens yapılarına kıyasla daha pratik ve düşük maliyetli çözümler geliştirilebilmektedir (Paraskevopoulos ve ark.,2022; Hoel ve ark.,2018). Özellikle düzlemsel ve radyal GRIN lens tasarımlarında faz eşitleme ve geometrik optik temelli yaklaşımlar öne çıkmaktadır. C-bantta dairesel kutuplu anten dizileriyle kullanılan 3B baskı uyumlu

GRIN lenslerde, farklı doluluk oranlarıyla radyal permitivite geçişi sağlanarak yaklaşık 4 dB kazanç artışı rapor edilmiştir (Paraskevopoulos ve ark.,2022). Benzer şekilde Ku-bantta geliştirilen radyal GRIN lens tasarımlarında, 3B baskı ile üretilen çok katmanlı yapının yüksek açıklık verimi ve yüksek yönlülük sağladığı deneysel olarak gösterilmiştir (Hoel ve ark.,2018). Ayrıca GRIN lenslerin sadece kazanç artırmak için değil, horn antenlerde yan lob seviyelerini düşürmek ve alan dağılımını iyileştirmek için de etkin biçimde kullanılabildiği gösterilmiştir (Urs ve ark.,2024). Bu yönleriyle 3B baskı tabanlı GRIN lensler, modern anten ve mikrodalga sistemleri için hafif, düşük maliyetli ve yüksek performanslı bir çözüm olarak değerlendirilmektedir. GRIN yaklaşımını tanımlamak için en basit ilişki eşitlik (1)'de verilmiştir. Burada $\boldsymbol{\eta}$ kırılma indisini, ε_r bağıl dielektrik sabitini ve μ_r bağıl manyetik geçirgenliği ifade etmektedir.

$$\boldsymbol{\eta} = \sqrt{\varepsilon_r \mu_r} \approx \sqrt{\varepsilon_r} \qquad (1)$$

Burada manyetik olmayan dielektrik yapılar için $\sqrt{\mu_r} \approx 1$, kabul edilir. Bu formül, kırılma indisinin etkin dielektrik sabitle ilişkisini verir.

2.2. Homojen ve Nonhomojen Lens Antenler

Lens antenler, elektromanyetik dalgaların faz cephesini kontrol ederek yüksek yönlülük, dar ışın genişliği ve gelişmiş kazanç elde etmeyi amaçlayan önemli anten yapıları arasında yer almaktadır. Bu yapılar genel olarak homojen ve nonhomojen lens antenler olmak üzere iki ana sınıfta incelenmektedir. Homojen lens antenlerde tüm lens hacmi boyunca dielektrik sabiti sabit kalırken, nonhomojen lens antenlerde kırılma indisi ya da eşdeğer dielektrik sabiti uzaysal olarak değişmektedir. Bu temel fark, hem elektromanyetik performans hem de üretim yaklaşımı açısından önemli tasarım ayrımlarını beraberinde getirmektedir (Chakrabarti ve ark.,2024; Lafond ve ark.2018).

Homojen lens antenler, görece daha basit geometrik tasarımları ve üretim kolaylıkları nedeniyle özellikle yüksek frekanslı haberleşme sistemlerinde yaygın olarak tercih edilmektedir. Örneğin D-bantta geliştirilen eliptik profilli homojen lens anten yapısında, tek bir dielektrik malzeme kullanılarak 142 GHz'de yaklaşık 32 dBi kazanç ve 3.2° × 3.2° yarı güç ışın genişliği elde edildiği rapor edilmiştir. Aynı çalışmada bu antenlerin iki uçta kullanılmasıyla görüş hattı haberleşme bağlantısında 55 Gbps veri iletimi deneysel olarak gösterilmiştir. Bu sonuçlar, homojen lens antenlerin özellikle milimetre dalga ve 6G aday bantlarında yüksek kazançlı, dar ışınlı ve uygulanabilir çözümler sunduğunu ortaya koymaktadır. Ayrıca homojen yapılarda yüzey profili uygun şekilde seçildiğinde küresel dalga cephesinin düzlemsel dalga cephesine dönüştürülmesi etkin biçimde sağlanabilmektedir (Chakrabarti ve ark.,2024).

Buna karşılık nonhomojen lens antenler, lens içerisinde merkezden kenara doğru değişen dielektrik sabiti dağılımı sayesinde daha hassas faz düzeltmesi yapabilmektedir. Özellikle Luneburg tipi lenslerde bu değişim, çok ışınlı çalışma ve geniş açılı tarama kabiliyeti sağlamaktadır. Ancak sürekli değişen permitivite dağılımının fiziksel olarak üretilmesi zordur. Bu nedenle literatürde, tek bir taban malzeme kullanılarak hava boşlukları, delikler, oluklar veya yoğunluk kontrollü yapılar yardımıyla etkin dielektrik sabiti ayarlanmış alternatif çözümler önerilmektedir. Silindirik Luneburg lensler üzerine yapılan karşılaştırmalı çalışmada, sabit dielektrik katsayılı bir malzemeye geometrik süreksizlikler eklenerek klasik katmanlı nonhomojen yapıya oldukça yakın elektromanyetik davranış elde edilebildiği gösterilmiştir (Korotkov ve ark.,2018).

Benzer şekilde, preslenmiş köpük tabanlı üretim yaklaşımında tek bir köpük malzemenin yoğunluğu değiştirilerek dielektrik sabitinin yaklaşık 1 ile 3 arasında ayarlanabildiği ve bu

yöntemle Luneburg ile Fresnel tipi nonhomojen lens antenlerin milimetre dalga bölgesinde başarıyla gerçekleştirilebildiği bildirilmiştir. Bu yöntemin düşük maliyetli, pratik ve milimetre dalga frekanslarına uygun olması önemli bir avantajdır. Sonuç olarak homojen lens antenler yapısal sadelik ve kolay üretim avantajı sunarken, nonhomojen lens antenler daha gelişmiş ışın şekillendirme, daha iyi faz kompanzasyonu ve çok ışınlı çalışma gibi üstün elektromanyetik özellikleriyle öne çıkmaktadır (Lafond ve ark.2018).

2.3. GRIN Lenslerde Temel Çalışma Prensibi

Gradient index (GRIN) lensler, elektromanyetik ya da optik dalgaların yayılımını, uzaysal olarak değişen kırılma indisi dağılımı yardımıyla kontrol eden yapılardır. Klasik homojen lenslerden farklı olarak bu yapılarda dielektrik sabiti ya da kırılma indisi lens boyunca sabit değildir; bunun yerine belirli bir radyal veya eksensel profile göre değiştirilir. Bu sayede lens içerisine giren farklı ışınların optik yol uzunlukları dengelenir ve çıkış yüzeyinde istenen faz dağılımı elde edilir. En temel amaç, bir noktasal ya da açıklık beslemesinden yayılan küresel dalga cephesini düzlemsel dalga cephesine dönüştürerek daha yüksek yönlülük ve kazanç sağlamaktır (Whiting ve ark.,2020;Songlin ve ark.,2018).

GRIN lenslerin çalışma mantığı büyük ölçüde faz eşitleme ve ışın-yolu dengeleme prensibine dayanır. Lensin merkezinden ve kenar bölgelerinden geçen ışınlar farklı geometrik mesafeler katettiği için, her bölgedeki etkin kırılma indisi uygun şekilde ayarlanarak tüm ışınların çıkış düzlemine yaklaşık aynı fazda ulaşması sağlanır. Böylece faz hatası azaltılır, enerji belirli bir doğrultuda toplanır ve dar huzmeli bir ışıma elde edilir. Bu tür yapılar dönüşüm optiği, geometrik optik ve dalga cephesi eşleme yaklaşımlarıyla tasarlanabilmektedir. Özellikle dönüşüm optiği, istenen elektromanyetik davranışın malzeme parametrelerine

gömülmesini sağlayarak GRIN lens tasarımına güçlü bir teorik temel sunmaktadır (Whiting ve ark.,2020).

Bunun yanında modern GRIN lens tasarımlarında topoloji optimizasyonu gibi ters tasarım yöntemleri de kullanılmaktadır. Bu yaklaşımda lens içerisindeki permitivite dağılımı, hedeflenen yönlülük veya alan dönüşümü için optimize edilmekte ve klasik yöntemlere göre daha yüksek performanslı çözümler elde edilebilmektedir (Songlin ve ark.,2018). Öte yandan, GRIN yapının tasarlanması kadar üretilen lensin kalite kontrolü de önemlidir. GRIN lens uç yüzeyindeki kusurların, yapı bütünlüğünün ve özellik dağılımının görüntü işleme temelli yöntemlerle incelenmesi, hedeflenen indeks profilinin pratikte doğru biçimde gerçekleştirilip gerçekleştirilmediğinin doğrulanmasına katkı sunmaktadır. Bu durum, GRIN lenslerin temel çalışma prensibinin yalnızca teorik indeks dağılımına değil, aynı zamanda bu dağılımın üretimde hassas biçimde korunmasına da bağlı olduğunu göstermektedir (Campbell ve ark.,2019).

2.4. Başlıca Performans Ölçütleri

Gradient Lens antenlerin ve özellikle GRIN tabanlı yapıların değerlendirilmesinde bazı temel performans ölçütleri öne çıkmaktadır. Bunların başında kazanç (gain) gelmektedir. Kazanç, antenin belirli bir yönde enerjiyi ne kadar etkin yoğunlaştırabildiğini gösterir ve lens kullanımının en önemli amaçlarından biri bu değeri artırmaktır. Bir diğer önemli ölçüt yönlülük (directivity) olup, ışımanın belirli bir doğrultuda ne kadar dar bir huzme şeklinde toplandığını ifade eder. Bununla bağlantılı olarak yarı güç huzme genişliği (HPBW) de değerlendirilir; daha küçük huzme genişliği genellikle daha yüksek yönlülüğe işaret eder.

Performans incelemelerinde ayrıca yan lob seviyesi (side lobe level) önemli bir kriterdir. Düşük yan lob seviyesi, enerjinin istenmeyen yönlere daha az yayılması anlamına gelir. Empedans

uyumu da temel ölçütlerden biridir ve genellikle yansıma katsayısı veya S_{11} parametresi ile değerlendirilir. İyi bir empedans uyumu, beslemeden antene daha fazla gücün aktarılmasını sağlar. Bunlara ek olarak verim (efficiency), çalışma bant genişliği, faz hatası, açıklık verimi ve bazı uygulamalarda ışın tarama kabiliyeti de lens antenlerin başarısını belirleyen önemli parametreler arasında yer almaktadır.

$$G = \mu D \tag{2}$$

$$\mu_{ap} = \frac{G\lambda^2}{4\pi A} \tag{3}$$

Burada "G" anten kazancını, "μ" anten verimini, "D" yönlülüğü, "μ_{ap}" açıklık verimini, "λ" dalga boyunu, "A" ise lensin fiziksel açıklık alanını ifade etmektedir. Eşitlik (2), anten kazancının yönlülük ve verim ile olan ilişkisini gösterirken, Eşitlik (3) açıklık veriminin kazanç, dalga boyu ve fiziksel açıklık alanına bağlı olarak nasıl tanımlandığını ortaya koymaktadır.

2.5. GRIN Lenslerin Modern Haberleşmedeki Önemi

GRIN lensler, modern haberleşme sistemlerinde yüksek kazanç, düşük profil, geniş bant genişliği ve gelişmiş ışın kontrolü gibi avantajları nedeniyle giderek daha fazla önem kazanmaktadır. Özellikle 5G, 6G, milimetre dalga ve terahertz tabanlı sistemlerde, elektromanyetik enerjinin belirli bir doğrultuda etkin biçimde yoğunlaştırılması kritik bir gereksinimdir. Bu noktada GRIN lens yapıları, klasik reflektör ve dizi anten çözümlerine alternatif olarak daha kompakt, hafif ve yüksek açıklık verimine sahip bir yaklaşım sunmaktadır. Dual-polarized GRIN metasurface lens anten çalışmasında, 10 GHz'de yaklaşık 15 dB kazanç, %60 bant genişliği ve 30 dB port izolasyonu elde edilmesi, bu yapıların çok kutuplamalı ve geniş bantlı haberleşme uygulamaları açısından güçlü bir aday olduğunu göstermektedir (Zega ve ark.,2022).

GRIN lenslerin önemi yalnızca RF ve mikrodalga haberleşme ile sınırlı değildir. Dalga odaklama ve enerji yoğunlaştırma kabiliyeti sayesinde bu yapılar, MEMS tabanlı enerji hasadı ve entegre dalga yönlendirme uygulamalarında da dikkat çekmektedir. Planar GRIN lensler üzerine yapılan çalışmada odak noktasında 7.49 kat büyütme elde edilmesi, uzaysal dalga kontrolünün ne kadar etkin gerçekleştirilebildiğini göstermektedir. Bu tür dalga manipülasyonu yetenekleri, gelecekte haberleşme ve algılama sistemlerinin daha küçük, verimli ve çok işlevli hâle gelmesine katkı sağlayabilir (Lin ve ark., 2020).

Ayrıca GRIN lenslerin asimetrik veya yön bağımlı indis profilleriyle ışın şekillendirme yapabilmesi, serbest uzay optik haberleşme gibi özel uygulamalarda da avantaj sağlamaktadır. Tek bir GRIN elemanıyla demet biçimlendirme ve kolimasyon yapılabilmesi, sistem karmaşıklığını azaltarak daha bütünleşik çözümler geliştirilmesine olanak tanımaktadır. Bu nedenle GRIN lensler, modern haberleşmenin yüksek performans, bütünleşme ve fonksiyonel esneklik gereksinimlerine cevap veren önemli yapılardan biri hâline gelmiştir (Sekh ve ark.,2012).

3. GRIN LENS YAPILARI VE UYGULAMALARI

3.1. Luneburg Lens Yapıları

Luneburg lens, merkezden dış yüzeye doğru değişen kırılma indisi profiline sahip klasik bir GRIN lens yapısıdır. Temel çalışma prensibi, bir noktadan yayılan küresel dalga cephesini düzlemsel dalga cephesine dönüştürmek veya tersine, düzlemsel dalgayı belirli bir odak noktasında toplamak üzerine kuruludur. Bu özellikleri sayesinde Luneburg lensler, yüksek kazanç, geniş açılı ışın tarama ve çok ışınlı çalışma gerektiren haberleşme ve radar sistemlerinde önemli bir yer tutmaktadır. İdeal Luneburg lens yapısında permitivite dağılımı küresel olarak

sürekli değişir; ancak bu profilin fiziksel olarak gerçekleştirilmesi zor olduğundan, pratikte katmanlı, ayrık hücreli ya da 3B baskı tabanlı eşdeğer yapılar kullanılmaktadır .

Son yıllarda geliştirilen Luneburg lens yapıları, yalnızca klasik küresel formda değil, ince, düzlemsel veya dönüştürülmüş geometrilerde de tasarlanmaktadır. Bu sayede daha düşük profil, daha kolay entegrasyon ve geniş bantlı çalışma gibi avantajlar elde edilmektedir. Ayrıca 3B baskı teknolojileriyle üretilen modern Luneburg lensler, çok ışınlı ve dairesel kutuplu anten uygulamalarında da başarılı sonuçlar vermektedir (Lei ve ark.,2022).

$$\varepsilon_r(r) = 2 - \left(\frac{r}{R}\right)^2 \tag{4}$$

$$\eta_r = \sqrt{2 - \left(\frac{r}{R}\right)^2} \tag{5}$$

Burada ε_r, lens içerisinde yarıçapa bağlı olarak değişen bağıl dielektrik sabitini, η_r ise buna karşılık gelen kırılma indisi dağılımını ifade etmektedir. Burada "r", lens merkezinden olan radyal uzaklığı, "R" ise lensin dış yarıçapını göstermektedir. Bu eşitlikler, Luneburg lens yapısında merkezden dış yüzeye doğru azalan indis profilinin dalga cephesini odaklama ve yönlendirme işlevini nasıl sağladığını ortaya koymaktadır.

3.2. Fresnel Lens Yapıları

Fresnel yapılar, klasik kalın lenslerin odaklama işlevini daha ince, hafif ve düşük hacimli bir geometriyle gerçekleştirmek amacıyla geliştirilmiştir. Temel prensip, sürekli lens profilinin eşfazlı bölgeler hâlinde bölünmesi ve böylece dalganın istenen odak noktasına yönlendirilmesidir. Bu yaklaşım, klasik kırıcı lenslere göre daha az malzeme kullanımı ve daha kolay üretim avantajı sağlamaktadır. Fresnel lenslerin analitik olarak modellenebilmesi ve sürekli profilin ayrık seviyelere dönüştürülebilmesi, tasarım ve üretim süreçlerini

kolaylaştırmaktadır. Ayrıca çok seviyeli ya da zonlu yapıların mikroüretim tekniklerine uygun olması, bu yapıların pratikte yaygınlaşmasını desteklemektedir.

Fresnel yapılar yalnızca optik sistemlerde değil, mikrodalga ve anten uygulamalarında da önemli bir yer edinmiştir. Özellikle 3B baskı ile üretilen dielektrik Fresnel lenslerde, farklı bölgelerde farklı etkin dielektrik sabitleri oluşturularak faz kompanzasyonu sağlanmakta ve yüksek yönlülük elde edilmektedir. 10 GHz için geliştirilen 3B baskılı dielektrik Fresnel lens tasarımında 18 dBi yönlülük elde edilmesi, bu yapıların anten uygulamaları açısından güçlü bir seçenek olduğunu göstermektedir. Bunun yanında Fresnel lens dizileri, integral görüntüleme gibi alanlarda da mikrolens dizilerine alternatif olarak önerilmekte; ancak kromatik sapma gibi etkiler bu yapılarda önemli bir tasarım parametresi olmaya devam etmektedir (Huang ve ark.,2015).

$$R_k = \sqrt{k\lambda f + \frac{\lambda^2 k^2}{4}} \tag{6}$$

Burada R_k, Fresnel lensin "k" bölgesine ait yarıçapı, "f"odak uzaklığını, "λ" çalışma dalga boyunu ve "k" ise zon numarasını ifade etmektedir. Bu eşitlik, Fresnel lens yapısında her bir bölgenin sınır yarıçapını belirlemek için kullanılmakta ve dalgaların odak noktasında uygun faz ilişkisiyle toplanmasını sağlamaktadır.

3.3. Mikaelian, Gutman ve Eaton Lens Yapıları

Mikaelian, Gutman ve Eaton lensler, klasik Luneburg lens dışında yer alan önemli GRIN lens türleri arasında bulunmaktadır. Mikaelian lens, dikdörtgensel ya da silindirik geometriye uygun yapısıyla öne çıkar ve özellikle düzlemsel dalga cephesini odaklama yeteneği sayesinde daha kompakt ve düşük profilli sistemlerin tasarımına imkân verir. Metayüzey tabanlı Mikaelian lenslerde, uzaysal olarak değişen indis dağılımı

kullanılarak odaklama başarımı sağlanırken, klasik dairesel lenslere göre daha ince ve dar yapı avantajı elde edilmektedir (Syue ve ark.,2016).

Gutman lens, Luneburg lensin daha genel bir formu olarak değerlendirilebilir. Bu yapıda odak yüzeyi lensin içine doğru kaydırılabilir ve özellikle kesilmiş (truncated) Gutman lens tasarımları sayesinde besleyici antenlerin düzlemsel bir yüzeye yerleştirilmesi mümkün hâle gelir. Bu özellik, çok ışınlı sistemlerde pratik entegrasyon avantajı sunmaktadır (Grigoriev ve ark.2022).

Eaton lens ise gelen dalgayı belirli bir açıyla saptırma özelliğiyle bilinir. Özellikle 90° ışın bükme yeteneği, bu lensi ışın yönlendirme ve beam deflection uygulamaları açısından değerli kılmaktadır. 3B baskı teknikleriyle gerçekleştirilen Eaton lens yapıları, GRIN profillerinin pratik olarak üretilebildiğini ve deneysel olarak doğrulanabildiğini göstermektedir (Du ve ark.,2016).

3.4. Gerçekleme Yöntemleri ve Üretim Yaklaşımları

GRIN ve dielektrik lens yapıların gerçekleştirilmesinde son yıllarda en dikkat çekici yöntemlerden biri 3B baskı teknolojileridir. Özellikle FDM, polymer jetting ve benzeri eklemeli üretim teknikleri sayesinde, uzaysal olarak değişen dielektrik sabiti profilleri pratik biçimde üretilebilmektedir. Bu amaçla genellikle tek bir taban malzeme kullanılarak doluluk oranı, hava boşluğu miktarı veya birim hücre geometrisi değiştirilmekte ve böylece farklı etkin permitivite değerleri elde edilmektedir. Bu yaklaşım, klasik işleme yöntemlerine göre hem maliyeti azaltmakta hem de karmaşık iç yapıların tek adımda üretilmesine imkân vermektedir.

Bunun yanında lens üretiminde yalnızca elektromanyetik uygulamalar değil, optik ve ultrasonik sistemler için geliştirilen mikroişleme, kontrollü kazıma ve özel kalıplama teknikleri de

önem taşımaktadır. Uygulamaya bağlı olarak yüzey profili oluşturma, zonlu yapı üretimi, birim hücre tabanlı yapılandırma ve doğrudan hacimsel üretim gibi farklı yöntemler tercih edilmektedir. Sonuç olarak modern üretim yaklaşımları, lens yapıların daha hafif, düşük maliyetli, hızlı prototiplenebilir ve uygulamaya özel biçimde gerçekleştirilmesini mümkün kılmaktadır. Tablo 1' de bu kitap bölümünde geçen GRIN lens türlerinin genel bir karşılaştırmalı özeti verilmiştir.

Tablo 1. Başlıca GRIN lens yapılarının genel performans ve yapısal özellik karşılaştırması

Lens Türü	İndis Yapısı	Geometri	Işın Tarama	Üretim Zorluğu	Yapısal Avantaj
Luneburg Lens	Sürekli gradyan indisli	Genellikle küresel	Çok uygun	Orta-yüksek	Geniş açılı tarama ve çoklu besleme ile çalışma
Fresnel Lens	Bölgesel	İnce ve düzlemsel yapı	Sınırlı-orta	Düşük-orta	Düşük profil, hafiflik ve az malzeme kullanımı
Mikaelian Lens	Gradyan indisli	Dikdörtgensel	Sınırlı	Orta	Kompakt ve dar yapılı sistemlere uygunluk
Gutman Lens	Gradyan indisli	Kesilmiş veya iç odaklı yapı	Uygun	Orta-yüksek	Düzlemsel besleme yerleşimine daha elverişli olması
Eaton Lens	Gradyan indisli	Genellikle dairesel	Yön saptırma odaklı	Yüksek	Işın bükme ve yön değiştirme kabiliyeti

4. SONUÇLAR

Bu bölümde GRIN lens yapıları, temel çalışma prensipleri, başlıca lens türleri ve modern haberleşme uygulamalarındaki rolleri genel bir çerçevede ele alınmıştır. Homojen ve inhomojen lens yapılar arasındaki farklar incelenmiş, özellikle GRIN lenslerin uzaysal olarak değişen kırılma indisi profilleri sayesinde elektromanyetik dalgaların fazını ve yayılım yönünü etkin biçimde kontrol edebildiği vurgulanmıştır. Luneburg, Fresnel, Mikaelian, Gutman ve Eaton gibi farklı lens türleri; odaklama, ışın yönlendirme, çok ışınlı çalışma ve düşük profilli tasarım açısından sundukları avantajlar bakımından değerlendirilmiştir.

Ayrıca, bu yapıların gerçekleştirilmesinde kullanılan üretim yaklaşımlarının da son yıllarda önemli ölçüde geliştiği görülmektedir. Özellikle 3B baskı teknolojileri, GRIN lenslerin daha düşük maliyetle, daha hafif ve uygulamaya özel biçimde üretilebilmesini mümkün kılmıştır. Bu durum, lens antenlerin yalnızca teorik araştırma konusu olmaktan çıkıp pratik mühendislik uygulamalarında daha yaygın biçimde kullanılmasına zemin hazırlamıştır.

Sonuç olarak GRIN lensler, yüksek kazanç, gelişmiş ışın kontrolü, geniş bant potansiyeli ve kompakt yapı avantajlarıyla modern haberleşme sistemleri için güçlü bir çözüm sunmaktadır. Gelecekte 5G/6G, milimetre dalga, radar ve uydu haberleşme sistemlerinde bu yapıların daha fazla önem kazanacağı öngörülmektedir.

KAYNAKÇA

Arican, G. O., Dokmetas, B., Akcam, N., & Yazgan, E. (2019). 28–36 GHz MMIC LNA design for satellite applications. In 2019 11th International Conference on Electrical and Electronics Engineering (ELECO) (pp. 726–729). Bursa, Turkey.

Campbell, S. D., Werner, D. H., & Werner, P. L. (2019). Transformation optics and related techniques for GRIN lens design. In 2019 13th European Conference on Antennas and Propagation (EuCAP) (pp. 1–3). Krakow, Poland.

Chakrabarti, S., Singh, V. K., Kumar, A., Thomas, K. G., & Rao, P. H. (2024). High gain elliptic lens antenna at D-band for 6G multi Gbps data transmission. In 2024 IEEE International Symposium on Antennas and Propagation and INC/USNC-URSI Radio Science Meeting (AP-S/INC-USNC-URSI) (pp. 887–888). Firenze, Italy.

Dokmetas, B., & Arican, G. O. (2023). Design of dual-band SIW antenna for millimeter-wave communication. In Proceedings of the 31st Telecommunications Forum (TELFOR) (pp. 1–4).

Dokmetas, B., Arican, G. O., & Yilmaz, B. A. (2024). A folded pyramid-shaped microstrip antenna with improved bandwidth. In Proceedings of the 2024 IEEE International Symposium on Antennas and Propagation and ITNC-USNC-URSI Radio Science Meeting (AP-S/INC-USNC-URSI) (pp. 1273–1274). Firenze, Italy.

Dokmetas, B., Arican, G. O., Akcam, N., & Yazgan, E. (2019). A novel millimeter-wave U-shaped radiating slot antenna with DGS structures for 5G cellular application. In 2019 11th International Conference on Electrical and

Electronics Engineering (ELECO) (pp. 669–672). Bursa, Turkey.

Du, G., Liang, M., Sabory-Garcia, R. A., Liu, C., & Xin, H. (2016). 3-D printing implementation of an X-band Eaton lens for beam deflection. IEEE Antennas and Wireless Propagation Letters, 15, 1487–1490.

Grigoriev, I., & Munina, I. (2022). Multibeam truncated Gutman lens based on additive manufacturing. In 2022 International Workshop on Antenna Technology (iWAT) (pp. 104–106). Dublin, Ireland.

Hoel, K. V., Kristoffersen, S., Ignatenko, M., & Filipovic, D. (2018). Half ellipsoid Luneburg GRIN dielectric lens loaded double ridged horn antenna. In 12th European Conference on Antennas and Propagation (EuCAP 2018) (pp. 1–5). London, UK.

Huang, C.-Y., Li, J.-H., Chiou, P.-C., & Chung, T.-T. (2015). Fresnel lens array with chromatic dispersion for integral imaging. In 2015 IEEE 5th International Conference on Consumer Electronics - Berlin (ICCE-Berlin) (pp. 452–455). Berlin, Germany.

Korotkov, A., & Mitelman, Y. (2018). Comparison of Luneburg lens antennas made from homogeneous material. In 2018 Ural Symposium on Biomedical Engineering, Radioelectronics and Information Technology (USBEREIT) (pp. 334–337). Yekaterinburg, Russia.

Lafond, O., Himdi, M., Bor, J., & Jouadé, A. (2018). Inhomogeneous lens antenna using pressed foam technological process in MM wave range. In 2018 IEEE Conference on Antenna Measurements & Applications (CAMA) (pp. 1–4). Sweden.

Lei, S., Wei, G., Han, K., Li, X., & Qiu, T. (n.d.). A wideband 3-D-printed multibeam circularly polarized ultrathin dielectric slab waveguide Luneburg lens antenna. IEEE Antennas and Wireless Propagation Letters, 21(8), 1582–1586.

Lin, Q.-W., To, Y.-S., & Wong, H. (2020). A dual-polarized lens antenna using gradient refractive index (GRIN) metasurface. In 2020 IEEE Asia-Pacific Microwave Conference (APMC) (pp. 1063–1065). Hong Kong.

Paraskevopoulos, A., Gashi, I., Albani, M., & Maci, S. (2022). High aperture efficiency 3D-printed radial GRIN lens. In 2022 16th European Conference on Antennas and Propagation (EuCAP) (pp. 1–5). Madrid, Spain.

Sekh, M. A., Sarkar, S. K., SoodBiswas, N., & Basuray, A. (2012). Correcting beam astigmatism in laser diode by the use of single anamorphic GRIN lens. In 2012 5th International Conference on Computers and Devices for Communication (CODEC) (pp. 1–3). Kolkata, India.

Songlin, W., Min, Z., Bo, Z., Lei, D., & Qian, Y. (2018). Image processing methodology for features extraction of GRIN lens end. In 2018 IEEE International Conference of Safety Produce Informatization (IICSPI) (pp. 458–461). Chongqing, China.

Syue, C. J., Kehn, M. N. M., & Quevedo-Teruel, O. (2016). Compact Mikaelian lens design using metasurface structure. In 2016 International Symposium on Antennas and Propagation (ISAP) (pp. 534–535). Okinawa, Japan.

Urs, J. K. P., Amogh, G., & Shushrutha, K. S. (2024). 3D printable GRIN lens for C-band circularly polarized antenna. In 2024 IEEE Microwaves, Antennas, and

Propagation Conference (MAPCON) (pp. 1–4). Hyderabad, India.

Whiting, E. B., et al. (2020). Topology optimization of RF GRIN lenses. In 2020 IEEE International Symposium on Antennas and Propagation and North American Radio Science Meeting (pp. 101–102). Montreal, QC, Canada.

Zega, V., Antonacci, M., Frangi, A., Corigliano, A., & Riva, E. (2022). Planar GRIN lenses for MEMS energy harvesters: A macroscale proof of concept. In 2022 Joint Conference of the European Frequency and Time Forum and IEEE International Frequency Control Symposium (EFTF/IFCS) (pp. 1–4). Paris, France.

ARTIFICIAL INTELLIGENCE FOR RESILIENT MICROGRIDS AND SMART GRIDS: FROM PREDICTION TO AUTONOMOUS ENERGY MANAGEMENT[1]

Seyfullah DEDEOĞLU[2]

1. INTRODUCTION

The power sector is being reshaped by three developments that are unfolding at the same time: the rapid growth of renewable generation, the proliferation of distributed energy resources, and the digitalization of grid operation. These shifts have turned the electricity network into a data-intensive cyber-physical system in which sensing, communication, forecasting, optimization, and control can no longer be treated as loosely connected functions. The smart-grid vision described by Amin and Wollenberg (2005) and later synthesized in the survey by Fang et al. (2012) anticipated exactly this transformation: a power system that is observable, adaptive, and able to coordinate millions of heterogeneous devices without sacrificing reliability.

Microgrids are central to this transition because they organize distributed assets into controllable local energy cells. A microgrid typically combines renewable generation, dispatchable units, energy storage, flexible loads, and power electronic interfaces that can operate either in coordination with the main

---

[1] This chapter was prepared as an original contribution for this edited volume and was not adapted from a previously published thesis or conference paper.

[2] Assistant Prof., Hitit University, Faculty of Engineering and Natural Sciences, Department of Electrical-Electronics Engineering, ORCID: 0000-0001-7969-011X.

network or in islanded mode when resilience is required. Lasseter's seminal formulation of the microgrid concept and the influential overview of Hatziargyriou et al. (2007) made it clear that the value of microgrids lies not only in local generation, but in coordinated intelligence. Once a microgrid contains photovoltaic systems, batteries, electric vehicles, demand response resources, and converter-dominated dynamics, conventional rule-based supervision becomes increasingly fragile.

Artificial intelligence has therefore moved from a peripheral analytical tool to an operational enabler for both smart grids and microgrids. In practice, AI is not a single technique but a family of methods used to extract structure from large volumes of data, support forecasting under uncertainty, detect abnormal behavior, learn control policies, and assist operators in complex decision environments. Recent reviews confirm that AI is now being applied across forecasting, protection, energy management, fault diagnosis, restoration, and cybersecurity tasks in distribution-level and local-area grids (Ali & Choi, 2020; Ibrahim, Dong, & Yang, 2020; Mohammadi et al., 2022; Joshi et al., 2023).

This chapter examines how AI is being used in smart-grid and microgrid technologies from an engineering perspective. The discussion focuses on the applications that matter most in practice: forecasting, state awareness, anomaly detection, demand flexibility, energy management, resilient operation, and converter-dominated control. Rather than treating AI as a fashionable add-on, the chapter positions it as a decision-support and autonomy layer that must coexist with power-system physics, regulatory obligations, and operator oversight. The chapter also highlights why the next wave of progress is likely to come from hybrid approaches that integrate machine learning with optimization, digital twins, and physics-informed modeling.

2. THE STRATEGIC ROLE OF AI IN MODERN GRID ARCHITECTURES

2.1. Smart Grids as Data-Rich Cyber-Physical Energy Systems

Smart grids and microgrids are often discussed together, but they differ in scope and operational granularity. The smart grid refers to the modernization of the wider electricity system through advanced metering, two-way communication, distributed monitoring, flexible demand, automation, and data-enabled coordination. Microgrids, by contrast, are localized subsystems capable of self-management within a defined electrical boundary. The distinction matters because AI is not deployed at a single layer. Some applications, such as feeder-level load forecasting or asset health monitoring, belong naturally to the smart-grid domain. Others, such as battery dispatch, converter coordination, or islanding support, are more naturally framed at the microgrid level.

AI becomes strategically important when it reduces this dimensionality without hiding the operational meaning of the result. In a smart grid, for example, probabilistic load forecasting can transform raw meter, weather, and calendar data into uncertainty-aware demand envelopes that are directly usable in scheduling and congestion management. In a microgrid, the same logic applies to net-load prediction, photovoltaic output estimation, battery state-of-charge trajectory modeling, and real-time flexibility assessment. These are not abstract analytics tasks; they determine whether the system buys energy at the right time, preserves reserve margins, avoids unnecessary cycling, and rides through disturbances with acceptable service continuity.

A second strategic role of AI lies in converting dense measurement streams into situational awareness. Future grids will rely increasingly on synchronized phasor data, smart inverter

telemetry, power quality measurements, weather nowcasts, and event logs from protection and automation devices. Huang et al. (2012) emphasized that state estimation in the future grid would face new challenges linked to scale, heterogeneity, and incomplete observability. AI does not replace estimation theory, but it strengthens it by learning latent patterns, correcting biases, flagging inconsistent data, and prioritizing human attention toward events that matter.

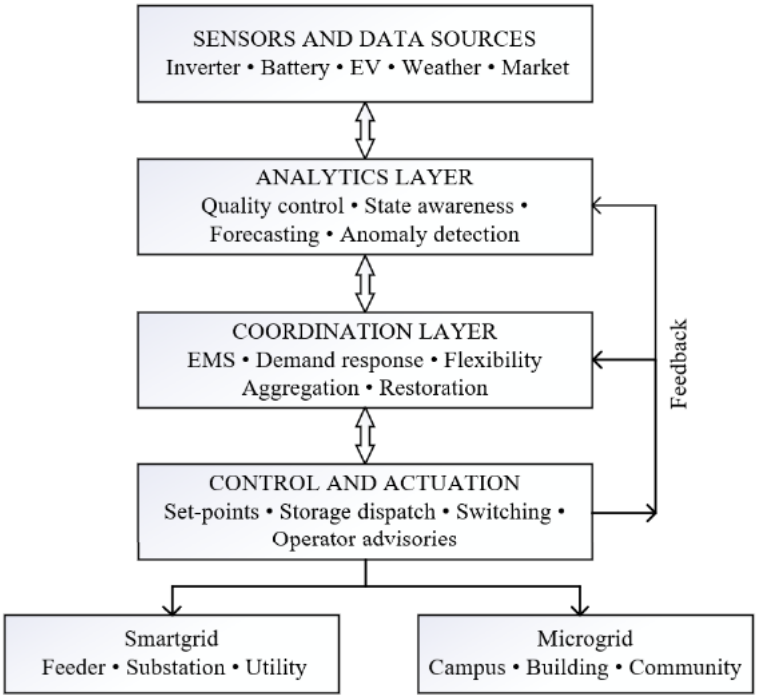

Figure 1. Layered architecture of AI-enabled coordination in smart grids and microgrids.

2.2. Microgrids as Controllable Local Energy Cells

A third role concerns control across multiple time scales. In converter-dominated systems, the operational objectives of a microgrid range from millisecond stability support to minute-level balancing and day-ahead economic scheduling. The

influential work of Guerrero et al. (2011) on hierarchical control and the later review by Olivares et al. (2014) showed that microgrid operation is inherently layered. AI fits naturally into this layered structure. It is strongest at the supervisory, predictive, and coordination layers, where uncertainty, nonlinear interactions, and combinatorial decisions dominate, while classical control remains indispensable in the innermost loops where timing guarantees and stability margins are paramount.

For this reason, the most productive way to think about AI in energy is not as an alternative to power engineering, but as an intelligence layer embedded within a broader architecture of sensing, estimation, optimization, and actuation. Figure 1 illustrates this architecture and highlights how AI links operational data to decisions at system, feeder, and microgrid levels.

3. AI METHODS THAT MATTER FOR GRID OPERATION

3.1. Supervised and Deep Learning for Prediction

The breadth of AI techniques used in power and energy systems can be reduced to a few operationally meaningful categories. The first category is supervised learning, which includes linear and nonlinear regression, decision trees, support vector methods, ensemble learners, and deep neural networks. These methods are especially effective when the goal is to approximate an input-output mapping from historical data. In grid contexts, they are used for load forecasting, photovoltaic generation forecasting, electricity price estimation, transformer health prediction, battery degradation assessment, and power quality classification. Their appeal lies in their flexibility: they can exploit high-dimensional covariates such as weather

forecasts, occupancy patterns, market variables, and device telemetry without requiring full first-principles modeling.

3.2. Unsupervised Learning and Event Discovery

The second category is unsupervised and semi-supervised learning, which is useful when labeled fault or event data are scarce. Clustering methods support consumer segmentation, tariff design, and flexibility characterization. Dimensionality reduction methods help operators visualize latent operational regimes. Autoencoders and density-based anomaly detectors are increasingly used to detect cyber intrusions, meter tampering, incipient equipment failures, or unusual operating points in inverter-rich networks. These approaches are particularly valuable in power systems because abnormal conditions are rare by definition, and fully labeled datasets are often unavailable or costly to curate.

3.3. Reinforcement Learning, Hybrid Intelligence, and Explainability

The third category is sequential decision making, especially reinforcement learning. This is one of the most attractive AI paradigms for microgrids because energy management is inherently a closed-loop control problem under uncertainty. At each time step, the controller must decide how to dispatch storage, flexible demand, controllable generation, or market exchanges based on current measurements and expectations about the future. Reinforcement learning can, in principle, learn these policies directly from interaction data or simulation. The well-known work of Ruelens et al. (2017) demonstrated the promise of batch reinforcement learning for residential demand response, and similar ideas have since been extended to storage scheduling, building flexibility, electric vehicle coordination, and microgrid dispatch.

Still, unrestricted learning is not acceptable in safety-critical energy infrastructure. A practical deployment must account for constraint violations, action feasibility, model uncertainty, and fallback logic. This is why hybrid approaches are gaining traction. A learned forecasting model may feed a mixed-integer optimizer. A reinforcement learning agent may operate inside a supervisory envelope defined by rule-based safety constraints. A neural estimator may run alongside a physics-based observer. Increasingly, the question is not which single method wins, but how data-driven intelligence can be embedded in a verifiable decision pipeline.

4. AI APPLICATIONS IN SMART GRIDS

4.1. Forecasting, Flexibility, and Demand Response

Forecasting remains the most mature and economically consequential AI application in smart grids. Grid operators need accurate predictions of load, renewable generation, price, reserve needs, and congestion risk across horizons ranging from minutes to days. Hong and Fan (2016) provided a highly cited tutorial on probabilistic electric load forecasting that helped shift the conversation away from single-point predictions toward uncertainty-aware methods. This shift is essential. In modern grids, decisions are rarely made on the basis of a single expected value; they depend on quantiles, confidence intervals, ramp risk, and the likelihood of extreme deviations. AI contributes by learning nonlinear weather-demand relationships, holiday effects, occupancy signatures, and feeder-specific consumption patterns.

The integration of demand response adds a second layer of complexity. In conventional scheduling, demand was largely treated as exogenous. In smart grids, responsive demand becomes a controllable resource whose flexibility depends on user comfort, appliance states, price signals, and behavioral uncertainty.

Siano's influential survey (2014) demonstrated how demand response evolved into a central smart-grid mechanism for balancing variability and improving system efficiency. AI methods now support customer segmentation, response forecasting, dynamic pricing design, and the aggregation of distributed flexibility portfolios. When carefully deployed, these methods reduce peak demand, defer network reinforcement, and improve the absorption of variable renewable generation.

4.2. State Awareness, Asset Analytics, and Anomaly Detection

At the distribution level, AI is also transforming state awareness. Classical state estimation remains indispensable, but smart grids face observability gaps, asynchronous measurements, and data quality issues that are difficult to handle with purely model-based techniques. Machine learning helps by identifying bad data, imputing missing values, inferring latent load behavior, and accelerating estimation in large networks. Huang et al. (2012) anticipated many of these challenges in the future grid. The practical contribution of AI here is not to replace the physics of power flow, but to improve robustness when measurements are sparse, delayed, or corrupted.

Condition monitoring and predictive maintenance form another major application domain. Smart grids contain a vast asset base, including transformers, cables, circuit breakers, relays, meters, switchgear, and converter-based interfaces. Maintenance policies based solely on fixed intervals can be both expensive and inadequate. AI models trained on temperature profiles, dissolved gas analysis, partial discharge signatures, harmonics, vibration, and event logs can identify degradation patterns before they evolve into failures. The value is greatest when these predictions are tied to maintenance prioritization, spare-parts planning, and

outage-risk assessment rather than treated as isolated classification outputs.

4.3. Cybersecurity and Planning Intelligence

Cybersecurity is now impossible to separate from operational reliability. Smart grids expose a larger attack surface because sensors, distributed controllers, cloud services, market interfaces, and edge devices all contribute to the control loop. AI supports intrusion detection, log correlation, and anomaly scoring across cyber-physical datasets, but it also introduces new vulnerabilities such as adversarial manipulation, data poisoning, and model drift. The deployment lesson is clear: AI should strengthen defense-in-depth, not become a single point of failure. Secure architectures require authenticated data paths, role-based access control, model versioning, and independent operational safeguards that continue to function even when the analytics layer is compromised.

5. AI APPLICATIONS IN MICROGRIDS

5.1. Energy Management and Economic Dispatch

If the smart grid is the macro-level expression of digital energy, the microgrid is its most experimentally rich local manifestation. A microgrid concentrates many of the operational challenges of the future power system into a bounded environment: renewable intermittency, converter interactions, storage scheduling, flexible demand, limited inertia, islanding capability, and multiobjective decision making. This is why AI has found especially fertile ground in microgrids. The question is seldom whether a microgrid should be optimized, but how often, with what information, under which constraints, and at what level of autonomy.

The most visible application is energy management. Microgrid energy management systems must decide how to schedule dispatchable units, charge or discharge storage, shift flexible demand, manage imports and exports, and preserve operational reserves. The objective may be cost minimization, emission reduction, resilience improvement, battery life preservation, or some weighted combination of these goals. AI contributes in two complementary ways. First, it improves the forecasts on which scheduling depends. Second, it can learn or assist the supervisory policy itself. Reviews by Mohammadi et al. (2022) and Joshi et al. (2023) show that machine learning is increasingly used to support or replace heuristic energy management rules in systems with diverse distributed resources.

A robust microgrid scheduler must anticipate not only expected conditions but also uncertainty propagation. For example, a battery dispatch plan that appears optimal under mean photovoltaic output may become fragile if cloud cover is underestimated or a flexible load does not respond as expected. AI-based scenario generation and probabilistic prediction are therefore highly valuable. They allow the energy management layer to preserve flexibility for later intervals rather than greedily optimizing the current step. In practice, this often leads to better resilience and less aggressive cycling of storage assets.

Reinforcement learning is particularly attractive for these supervisory tasks because it treats the scheduler as a sequential decision maker. Instead of solving each step independently, the controller learns how current actions influence future opportunities and penalties. This is well aligned with battery management, thermal flexibility, and tariff-sensitive operation. Nevertheless, the raw version of reinforcement learning is rarely sufficient for field deployment. The operationally meaningful variants are those embedded in safe exploration rules, simulation-based pretraining, or optimization-informed action filters. When

reinforcement learning is combined with forecasts, state estimation, and constraint screening, it becomes a practical complement to model predictive or rule-based control rather than a speculative replacement.

5.2. Storage Scheduling, Electric Vehicles, and Local Flexibility

Electric vehicles add both complexity and opportunity to the microgrid. From an operator's perspective, EVs are mobile loads whose charging patterns may be synchronized, uncertain, and highly sensitive to pricing and user behavior. From an AI perspective, they are flexible storage-like resources with availability constraints. Learning-based methods can forecast arrival times, estimate departure energy needs, and coordinate charging to reduce peaks or absorb local renewable surplus. In campus, residential, and commercial microgrids, this capability can materially improve self-consumption rates and reduce stress on local transformers and converters.

5.3. Hierarchical Control and Islanded Operation

Beyond supervisory scheduling, AI increasingly supports secondary and tertiary control in inverter-dominated microgrids. The hierarchical framework established by Guerrero et al. (2011) remains highly relevant: primary control preserves immediate stability and power sharing, secondary control restores voltage and frequency, and tertiary control coordinates power flow and economic exchange with the upstream grid. AI contributes most strongly to secondary and tertiary layers, where prediction and adaptation matter. For instance, data-driven estimators can improve reference generation, disturbance classification, and the tuning of restoration actions after transients. However, the innermost converter loops should remain dominated by validated control laws whose stability properties are well understood.

This distinction is even more important in islanded operation. Islanded microgrids have reduced fault levels, tighter reserve margins, and greater sensitivity to measurement errors or control delays. A learned controller that behaves acceptably in grid-connected mode may become unstable when the network is islanded or weakly supported. The review by Olivares et al. (2014) remains instructive here: trends in microgrid control point toward greater intelligence, but also toward greater need for hierarchy and coordination. AI is most useful when it enhances preparedness and adaptation around these layers rather than bypassing them.

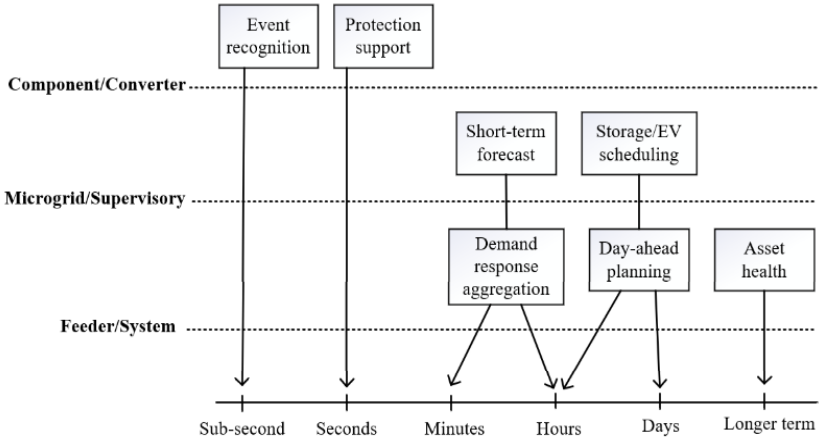

Figure 2. Mapping AI roles across grid and microgrid decision horizons.

5.4. Restoration, Resilience, and Market-Coupled Operation

Resilience and restoration constitute another promising frontier. After an outage, a microgrid must often decide how to re-energize segments, prioritize critical loads, sequence converter reconnection, and manage scarce local energy. These decisions are dynamic and conditional: the best action depends on evolving forecasts, available reserves, and component health. AI can

support restoration by ranking feasible switching plans, predicting post-restoration stress, and learning which recovery sequences preserve service quality with the lowest risk. In community microgrids, these capabilities may be as valuable as day-to-day economic optimization because they directly affect continuity of service for hospitals, communication systems, water infrastructure, and other critical loads. The decision horizons of those operations are summarized in Figure 2.

6. IMPLEMENTATION CHALLENGES AND DESIGN PRINCIPLES

6.1. Data Quality, Interoperability, and Compute Placement

Although the technical promise of AI in energy is substantial, deployment quality is determined by data quality, system integration, and governance. The first challenge is the gap between laboratory datasets and operational data streams. Utility and microgrid measurements are often missing, delayed, unsynchronized, or contaminated by communication faults and maintenance events. Labels may be sparse, especially for rare disturbances. A model that performs well on curated historical data can fail in production simply because the assumptions behind its features are not preserved. For this reason, data engineering, timestamp alignment, missing-value treatment, and model monitoring must be treated as part of the power-system design problem rather than as afterthoughts.

Interoperability is the second challenge. AI applications draw data from meters, phasor units, relays, building management systems, inverters, batteries, weather services, and market platforms that were rarely designed as a unified digital stack. Without careful data modeling and standardized interfaces, the cost of maintaining an AI application can exceed the value it

produces. The success of AI in smart grids therefore depends on robust middleware, semantic consistency, device metadata, and version-controlled feature pipelines. In practical terms, it is often more valuable to have a modest model fed by dependable data than a sophisticated model built on unstable interfaces.

6.2. Trust, Security, and Governance

Trust, explainability, and auditability are equally important. Operators need to understand why a model recommends a particular control action, and regulators need evidence that automated decisions are consistent with reliability obligations. This does not require every model to be simple, but it does require traceability. Inputs, assumptions, training data windows, validation procedures, and fallback strategies should all be documented. In many cases, the most reliable design is human-centered: AI generates ranked recommendations, confidence estimates, or scenario analyses, while the final action remains subject to supervisory approval or constraint screening.

Cybersecurity and privacy create another layer of complexity. Consumer-level load traces, behind-the-meter data, and distributed resource telemetry can reveal sensitive operational or behavioral information. Training centralized models on raw data is not always desirable or permissible. This is one reason federated learning, privacy-preserving aggregation, and edge analytics are attracting interest. At the same time, AI models themselves must be protected against unauthorized updates, model extraction, and adversarial inputs. Energy-sector digitalization cannot rely on blind trust in analytics vendors or cloud workflows; it requires a defensible security architecture that treats models as operational assets.

The final design principle is methodological humility. AI is powerful, but in power systems it must earn its place through repeatable validation, stress testing, and operational usefulness.

The best-performing solutions are usually hybrid: they preserve physical constraints, leverage domain structure, and remain interpretable enough to support maintenance, auditing, and lifecycle management.

7. FUTURE DIRECTIONS

The next phase of AI adoption in microgrids and smart grids will likely be shaped less by isolated benchmark accuracy and more by system-level integration. One major direction is the growing use of digital twins that couple physics-based simulation, historical data, and online telemetry. In such environments, AI models can be trained, stress-tested, and continuously updated against realistic operating conditions before they influence field decisions. This will be especially important for restoration planning, grid-forming converter coordination, and extreme-event preparedness.

Another direction is the rise of physics-informed and constraint-aware learning. As renewable penetration increases and microgrids become more converter dominated, the acceptable action space narrows. Learning algorithms that can internalize network equations, protection limits, and stability margins will be more valuable than generic black-box models. The same logic applies to reinforcement learning: safe and model-assisted variants are likely to dominate practical deployments because they align better with utility risk tolerance and certification requirements.

Finally, the field is moving toward decision intelligence rather than isolated prediction. The strongest AI systems will be those that connect forecasting, optimization, control, and post-event learning into a coherent operational loop. In other words, the future of AI in energy will not be defined by how many models are deployed, but by how effectively those models

improve reliability, resilience, efficiency, and transparency at scale.

8. CONCLUSION

Artificial intelligence is becoming a structural capability in modern power systems because smart grids and microgrids now operate in environments characterized by uncertainty, decentralization, dense sensing, and rapid decision cycles. The most valuable applications are not necessarily the most fashionable ones. Forecasting, demand flexibility, state awareness, anomaly detection, degradation assessment, and supervisory energy management already offer substantial operational benefits when they are integrated with sound engineering practice.

For microgrids in particular, AI adds value when it enhances local autonomy without undermining stability or safety. This means that AI should primarily strengthen supervisory, predictive, and coordination layers, while validated control methods continue to govern the innermost electrical dynamics. Smart-grid applications follow the same principle at a larger scale: learning systems should improve observability and decision quality, but they must remain compatible with physical constraints, cybersecurity requirements, and operator accountability.

The central lesson is therefore not that AI will replace conventional power-system methods, but that the future grid will be engineered through their combination. The most resilient architectures will merge measurement-rich digital infrastructures, domain-informed learning, hierarchical control, and transparent governance. In that combined form, AI can help transform smart grids and microgrids from reactive infrastructures into anticipatory and adaptive energy systems.

REFERENCES

Ali, S. S., & Choi, B. J. (2020). State-of-the-art artificial intelligence techniques for distributed smart grids: A review. Electronics, 9(6), 1030. doi:10.3390/electronics9061030

Amin, S. M., & Wollenberg, B. F. (2005). Toward a smart grid: Power delivery for the 21st century. IEEE Power and Energy Magazine, 3(5), 34-41. doi:10.1109/MPAE.2005.1507024

Fang, X., Misra, S., Xue, G., & Yang, D. (2012). Smart grid—The new and improved power grid: A survey. IEEE Communications Surveys & Tutorials, 14(4), 944-980. doi:10.1109/SURV.2011.101911.00087

Guerrero, J. M., Vasquez, J. C., Matas, J., de Vicuña, L. G., & Castilla, M. (2011). Hierarchical control of droop-controlled AC and DC microgrids—A general approach toward standardization. IEEE Transactions on Industrial Electronics, 58(1), 158-172. doi:10.1109/TIE.2010.2066534

Hatziargyriou, N., Asano, H., Iravani, R., & Marnay, C. (2007). Microgrids. IEEE Power and Energy Magazine, 5(4), 78-94. doi:10.1109/MPAE.2007.376583

Hong, T., & Fan, S. (2016). Probabilistic electric load forecasting: A tutorial review. International Journal of Forecasting, 32(3), 914-938. doi:10.1016/j.ijforecast.2015.11.011

Huang, Y.-F., Werner, S., Huang, J., Kashyap, N., & Gupta, V. (2012). State estimation in electric power grids: Meeting new challenges presented by the requirements of the future grid. IEEE Signal Processing Magazine, 29(5), 33-43. doi:10.1109/MSP.2012.2187037

Ibrahim, M. S., Dong, W., & Yang, Q. (2020). Machine learning driven smart electric power systems: Current trends and new perspectives. Applied Energy, 272, 115237. doi:10.1016/j.apenergy.2020.115237

Joshi, A., Capezza, S., Alhaji, A., & Chow, M.-Y. (2023). Survey on AI and machine learning techniques for microgrid energy management systems. IEEE/CAA Journal of Automatica Sinica, 10(7), 1513-1529. doi:10.1109/JAS.2023.123657

Lasseter, R. H. (2002). MicroGrids. In Proceedings of the IEEE Power Engineering Society Winter Meeting (Vol. 1, pp. 305-308). doi:10.1109/PESW.2002.985003

Mohammadi, E., Alizadeh, M., Asgarimoghaddam, M., Wang, X., & Simões, M. G. (2022). A review on application of artificial intelligence techniques in microgrids. IEEE Journal of Emerging and Selected Topics in Industrial Electronics, 3(4), 878-890. doi:10.1109/JESTIE.2022.3198504

Olivares, D. E., Mehrizi-Sani, A., Etemadi, A. H., Cañizares, C. A., Iravani, R., Kazerani, M., et al. (2014). Trends in microgrid control. IEEE Transactions on Smart Grid, 5(4), 1905-1919. doi:10.1109/TSG.2013.2295514

Ruelens, F., Claessens, B. J., Vandael, S., De Schutter, B., Babuska, R., & Belmans, R. (2017). Residential demand response of thermostatically controlled loads using batch reinforcement learning. IEEE Transactions on Smart Grid, 8(5), 2149-2159. doi:10.1109/TSG.2016.2517211

Siano, P. (2014). Demand response and smart grids—A survey. Renewable and Sustainable Energy Reviews, 30, 461-478. doi:10.1016/j.rser.2013.10.022

ELEKTRİK-ELEKTRONİK VE HABERLEŞME MÜHENDİSLİĞİ ALANINDA BİLİMSEL ARAŞTIRMALAR

yaz
yayınları

YAZ Yayınları
M.İhtisas OSB Mah. 4A Cad. No:3/3
İscehisar / AFYONKARAHİSAR
Tel : (0 531) 880 92 99
yazyayinlari@gmail.com • www.yazyayinlari.com